IOSR Journal of Electrical and Electronics Engineering (IOSR-JEEE)
ISSN: 2278-1676Volume 3, Issue 3 (Nov. - Dce. 2012), PP 01-07
www.iosrjournals.org

Dynamic compensation of reactive power in Various Faults in Power System

[1]R. K. Sampath, [2]C. Kumar
[1](Department of Electrical Engineering, p.v.p.siddhartha institute of technology, India)
[2](Department of Electrical Engineering, p.v.p.siddhartha institute of technology, India)

Abstract: *The STATCOM (Synchronous Static Compensator) based on voltage source converter (VSC) is used for voltage regulation in transmission and distribution system. The STATCOM can rapidly supply dynamic VARs required during system faults for voltage support. Strict requirements of STATCOM losses and total system loss penalty preclude the use of PWM (Pulse-Width Modulation) for VSC based STATCOM applications. This constraint of implementing VSC without PWM functionality, results in over-currents and trips of the STATCOM during and after system faults, when its VAR support functionality is most required. In this paper, we propose and develop an "emergency PWM" strategy to prevent over-currents (and trips) in the VSC during and after single line to ground system faults, LLLG faults and to ensure that the STATCOM supplies required reactive power. The Simulation results are shown for a 48-pulse VSC based ± 100 MVAR STATCOM connected to a 2- bus power strategy to prevent VSC over-currents and to supply required reactive power under line to ground system faults.*

Keywords: *STATCOM, Voltage Source Converter (VSC), Pulse-width Modulation (PWM), Single line to ground fault.*

I. Introduction

The Flexible AC Transmission systems (FACTS) controllers are emerging as an effective and promising alternative to enhance the power transfer capability and stability of the network by redistributing the line flow and regulating the bus voltages. Static VAR compensator (SVC) and Thyristor controlled series compensator (TCSC) are some of the commonly used FACTS controllers, The developments in the field of power electronics, particularly Gate Turn-off (GTO) based devices, have introduced a new family of versatile FACTS controllers, namely static synchronous compensator (STATCOM), The STATCOM is one of the custom power devices that received much attention for improving system stability, with the development of power electronics technology, custom power devices play important role in bringing unprecedented efficiency improvement and cost effectiveness in modern electrical power system [1,2]. The custom power is relatively new concept aimed at achieving high power quality, operational flexibility and controllability of electrical power systems [3-5]. The possibility of generating or absorbing controllable reactive power with various power electronic switching converters has long been recognized [6-8]. The STATCOM based on voltage source converter (VSC) is used for voltage regulation in transmission and distribution systems [8-12]. The STATCOM can rapidly supply dynamic VAR's during system faults for voltage support. In this paper, we propose and develop an "emergency PWM" strategy to prevent over-currents (and trips) in the VSC during line to ground faults, all though PWM technique results in higher switching losses but it recompense total system loss. This limitation of implementing VSC with PWM functionality, results in avoiding over-currents and trips of the STATCOM supplies required reactive power. With "emergency PWM" strategy STATCOM gains capability to prevent over-currents and trips in the VSC based STATCOM. Simulation results are presented for a 48-pulse VSC based ±100 MVAR STATCOM connected to a 2-bus power system. The operating characteristic of compensator during steady state, capacitive and inductive modes validate "emergency PWM" strategy [13] to prevent VSC over-currents and to supply required reactive power under line to ground system faults [9-12].

II. Vsc's Basic Structure

Fig. 1 shows the 48-pulse voltage source converter topology for ST ATCOM application. The VSC consists of four (lnv 1 - Inv4) 3-level Neutral Point Clamped (NPC) converters which are connected in series by four (Tl-T4) transformer coupling. The primary side of the transformer is connected in series as shown in Fig. 1. Due to the strict loss outlay for STATCOM application, each VSC is operated at fundamental frequency switching or in square-wave mode. The gating of VSCs is Phase-shifted so as to yield 48-pulse output voltage waveform with series transformer coupling on the primary side. The performance of the STATCOM under system faults (such as single line-ground faults) results in converter over currents and STATCOM trips.

Fig. 2 shows the phase B bus voltage dips for 4 cycles due to line-ground fault in the system. It has been noticed that primary STATCOM currents are large during system faults and results in ST ATCOM tripping. Examining further, it is seen that the VSCs "stop gating" during the fault due to over current strategy and enable the STATCOM to remain online, but cannot prevent the ST ATCOM trip recovering from the fault. It is realized that the VAR support functionality of the ST ATCOM is required the most during and after a system fault. This problem is the motivation for this work.

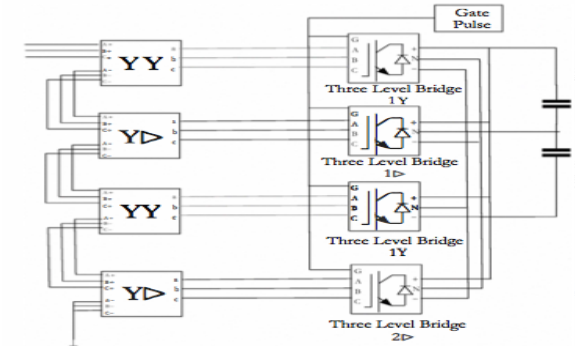

Figure. l The 48 –pulse voltage source converter circuit for ±100 MVA STATCOM application

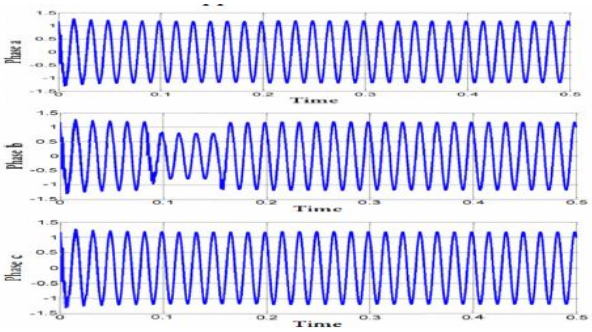

Figure.2 Performances under remote single line to ground fault resulting in phase b bus voltage sag

Fig.4 shows the 2-bus 500 kV power system simulation model with 48 pulses implemented VSC based ±100 MVAR STATCOM. Fig.4 shows the implemented angle controlled (α) STATCOM controller. An inner feedback loop is used to regulate the STATCOM instantaneous reactive power current Iq shunt, reminding that this control is achieved only by controlling α, of the inverter output voltage relative towards the transmission line voltage, this technique makes it possible to maintain a constant maximum ratio between the inverter Output voltage and the VSC dc-capacitor. The reference value for the reactive current control loop is generated by an outer loop responsible for the system voltage control (Vbus_ref). This outer control loop is similar to that used in conformist static VAR compensators, and includes an adjustable slope/droop setting that defines the voltage error at full STATCON reactive output. There is an unavoidable delay in the feedback of the voltage-regulating loop because of the time taken to compute the positive sequence fundamental bus voltage (Vbus). as a result an extremely fast response (typically 1⁄4 cycle) can be achieved for the reactive current controller (Iq. Shunt), the response time of the voltage regulator is typically about half Cycle of the line voltage.

III. Control Strategy

The proposed solution is based on "emergency PWM" mode, where the VSCs will individually detect and self implement PWM switching to control their phase (VSC pole and device) currents within predetermined limits. Each VSC will ensure that its over-current limit is not reached during and after a system fault, and under any bus voltage condition (including negative sequence and harmonics). This control strategy enables the STATCOM to remain online and recovering from a system fault, when its V AR support is required the most. Fig.6 and Fig.7 shows the VSC phase voltages and currents under normal and faulted conditions with "emergency pwm". The phase current rapidly increases at the onset of the fault and is typically higher than the over-current limit of the VSC devices. This "emergency PWM" concept is illustrated in such a way that the VSC phase voltage is modulated to control the phase (VSC pole and device) current during the fault. It is seen that the VSC phase current is controlled such that the STATCOM still delivers required reactive power (or current) during the fault. The extra switching's in the VSC will result in higher losses during this period. However, the priority is to keep the STATCOM online to support the bus voltage during and recovering from system faults.

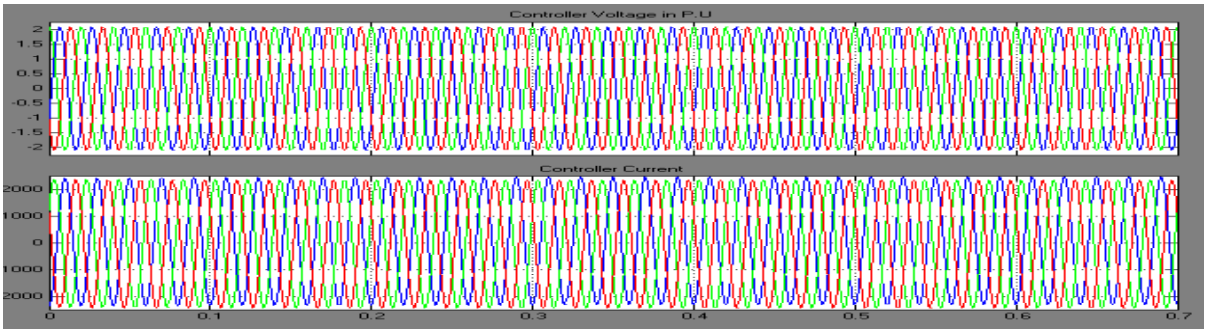

Figure.3 VSC phase voltage and current under normal condition

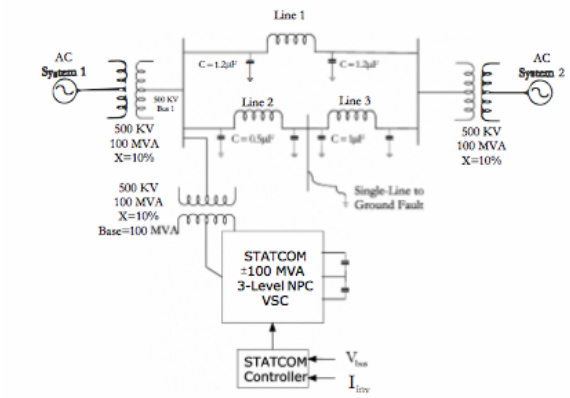

Figure.4 shows the 2-bus 500 kV power system simulation model with 48 pulses implemented VSC based ±100 MV AR STATCOM

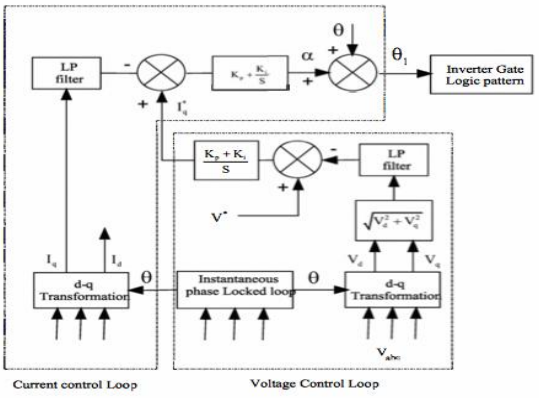

Figure. 5 STATCOM control block diagram

IV. Simulation Under Line To Ground And LLL-G Faults

The system simulation diagram is shown in Figure 4 with a 2-bus 500 kV power system. The ±100MV AR STATCOM is implemented with a 48-pulse VSC and is connected to a 500 kV bus as shown in Figure 3. A general fault generator is implemented at bus 2, which results in a voltage dip at the STATCOM bus. Attention is focused on single line-ground faults and STATCOM performance with the proposed "emergency PWM' concept in this section. Results given in per unit values, with 1.0 P.U as 500 kV. During steady state operation VSC voltage is in phase with system voltage. If the voltage generated by the VSC is higher (or lower) than the system voltage, then STATCOM generates (or absorbs) reactive power. The amount of reactive power depends on the VSC voltage magnitude and on the transformer leakage reactance. Varying dc bus voltage controls the fundamental component of VSC voltage. In order to vary dc voltage and therefore the reactive power, the VSC voltages angle (alpha), which is normally kept at close to zero, is now phase shifted. This VSC voltage may lag or lead and produces a temporary flow of active power, which results in, increase or decrease of dc capacitor voltages. With help of emergency pwm the output voltage distortion and capacitor ripple current can be reduced to any desired degree. Thus static VAR generator, employing a perfect voltage sourced converter, would produce sinusoidal output voltages, would draw sinusoidal reactive current from ac system

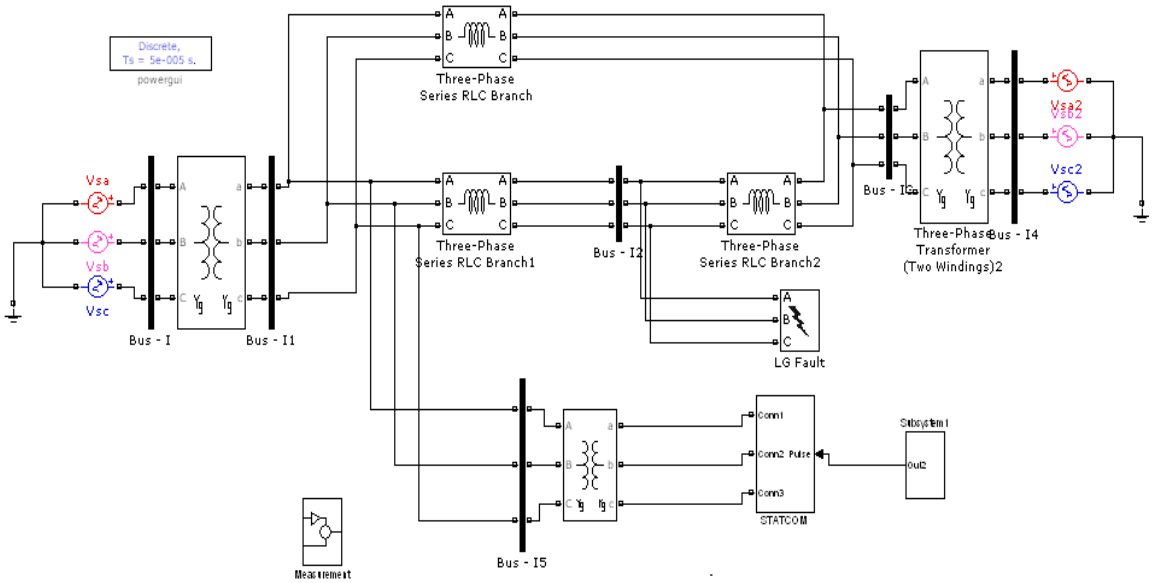

Fig.6 Simulink circuit of STATCOM connected system

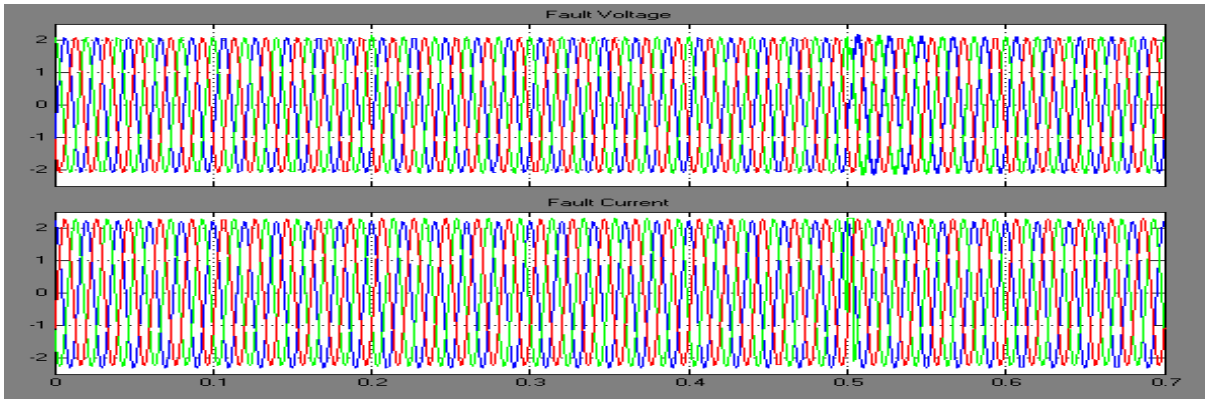

Figure 7 VSC voltage and current waveforms under normal condition

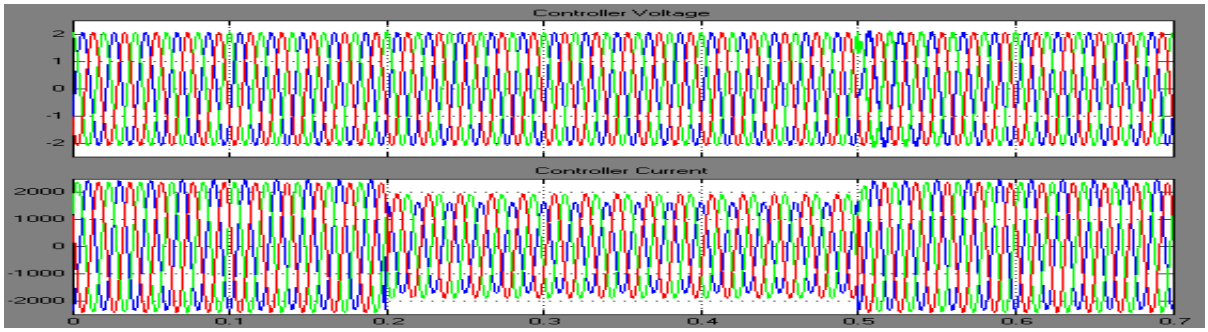

Figure.8.VSC voltage and current under LG fault

Fig.8 shows STATCOM operation in voltage regulation mode with emergency PWM under fault conditions. During fault conditions the inverter currents are very high this is the main reason for tripping and by implementing VSC with PWM functionality, avoids over-current and trips and in Fig. 8 It is clearly shown that bus voltage, injected currents are optimum, this ensures that STATCOM is in online and function without tripping, and from Fig. 8, we can examine continuous disparity in dc link voltage at 0.1 sec, during this period VAR output of STATCOM can change extremely rapidly, but the voltage controller takes time to determine the desired output, based on line voltage measurement. Once controller measures the desired voltage then STATCOM starts supplying reactive power to the load.

Under critical conditions. It is varying from inductive to capacitive within 0.2 to 0.3sec, which shows STATCOM supplying adequate reactive power under fault condition. Fig.9 shows the STATCOM controller voltages and currents, which are in permissible limits under fault conditions.

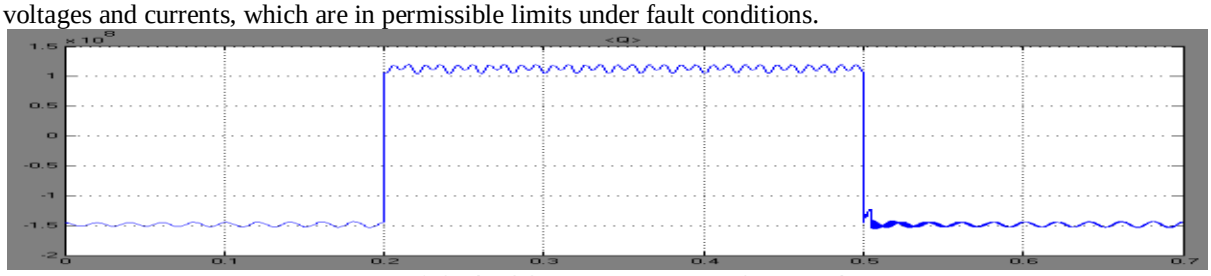

Figure.9 STATCOM reactive power Q in MVAR

STATCOM operates in two modes either capacitive are inductive mode, these are known according to Var variations. And dc link voltage always resembles STATCOM response; it is constant under normal stipulation. When ac voltage reduces STATCOM reacts fast and supplies necessary reactive power. At this condition reactive power Q is positive which resembles it is in capacitive mode, where as operation is vice versa when ac voltage increases.

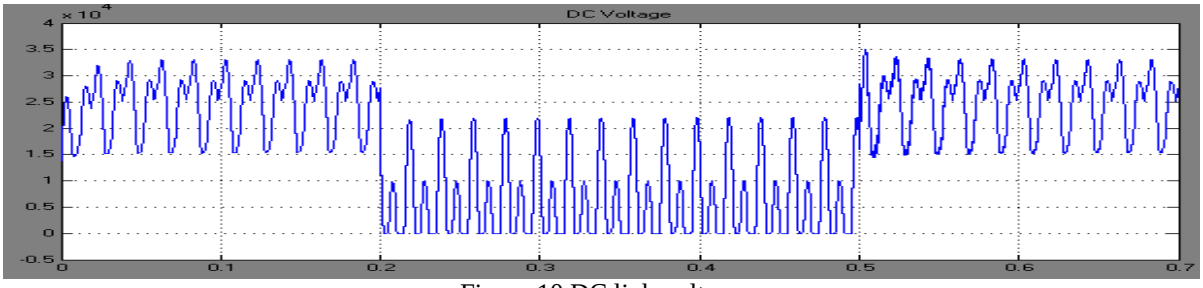

Figure.10 DC link-voltage

Figure.10 shows dc link voltage variations under normal operating conditions, in fact any change in dc link voltage represents variation in load.

V. LLL-G Fault

Fig.11 shows dynamic response of STATCOM under LLL-G faults, as these faults are sever, at this condition the inverters currents are very high than rated, but still STATCOM continuous to be in online without tripping and after a particular interval of time system comes to steady state. This is verified through Fig 11. The moment fault occurred, bus voltages start to fall but STATCOM responds abruptly and commence within minimum interval of time and starts supplying reactive power, these can be seen in Fig 13. From Fig.14, we can examine dc link voltage variations, under fault conditions and once STATCOM starts supplying then it gradually settles down i.e at point 0.2 sec, this signify

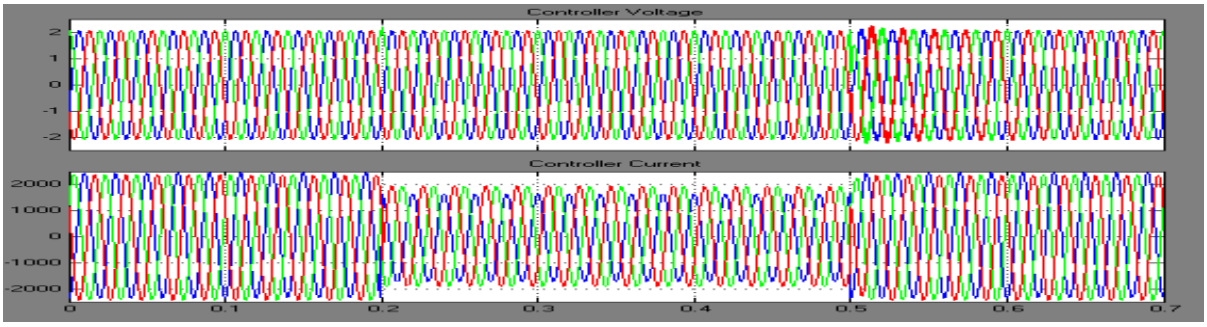

Figure. 11 VSC voltage and current under LLL fault

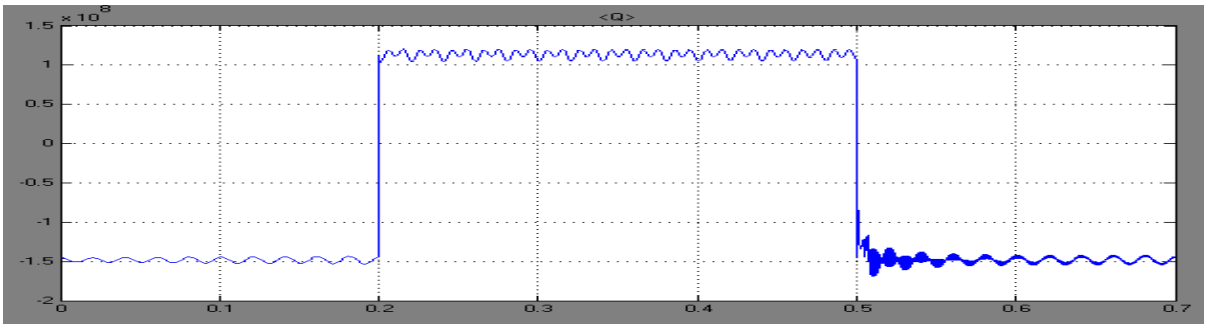

Figure. 12 STATCOM reactive powers Q in MVAR

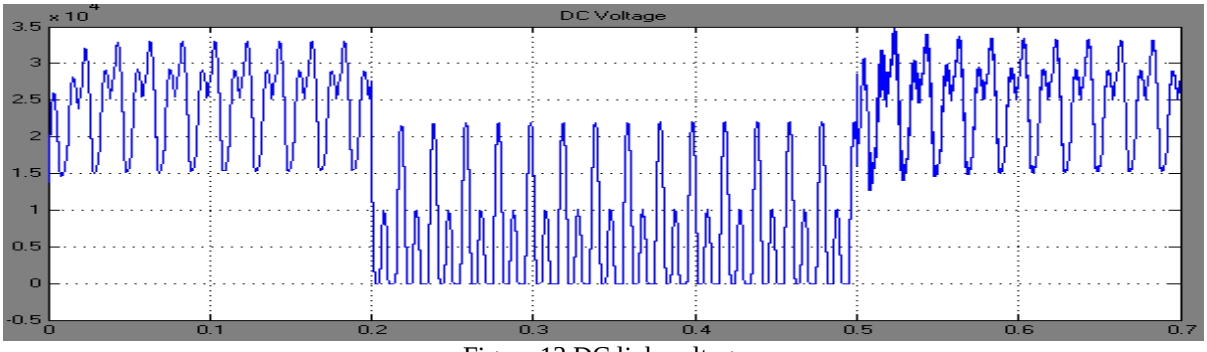

Figure.13 DC link-voltage

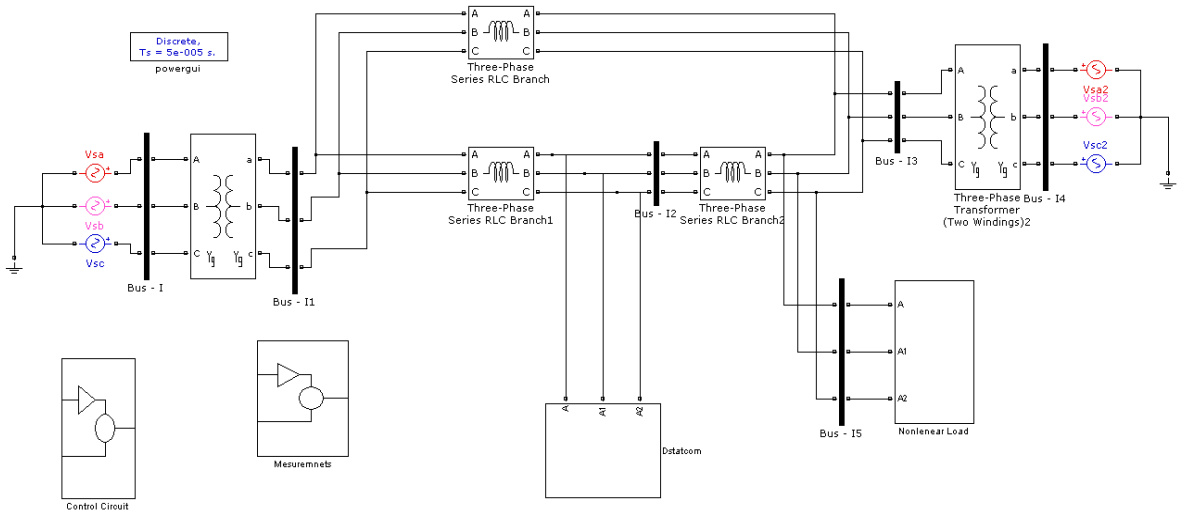

Fig.14 Simulation circuit of STATCOM connected to nonlinear load

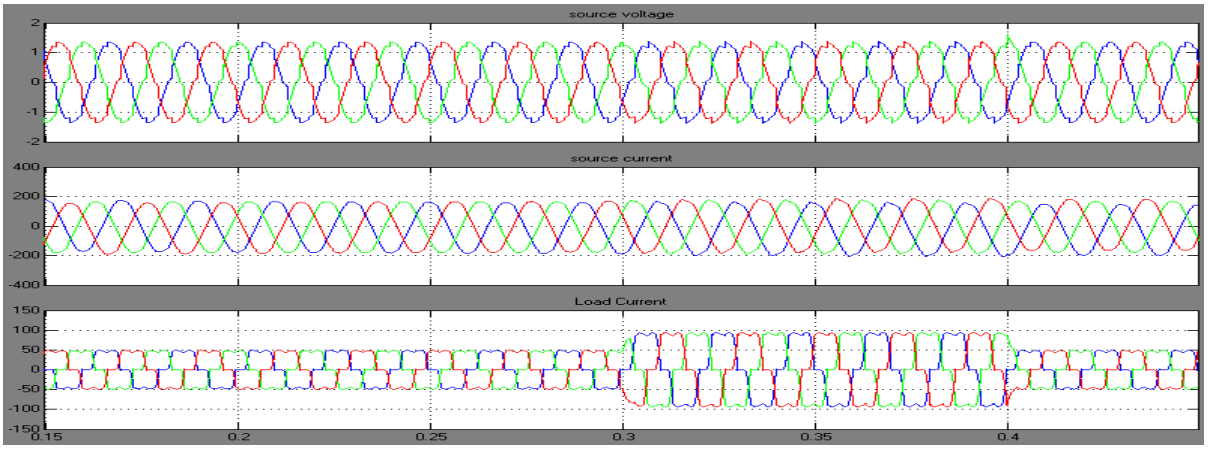

Fig.15 Source Voltage, current and Load current waveforms

Fig.14 shows the simulation circuit of the STATCOM connected to nonlinear load and Fig.15 shows the source voltage, current and the load current.

VI. Conclusion

This paper describes dynamic performance of STATCOM when it is subjected to L-G and LLL-G faults. The operating characteristic of compensator during steady state, capacitive and inductive modes of operation has been reasonably acceptable and competitive for design of an economical dynamic static compensator and by implementing "emergency PWM" strategy STATCOM gains capability to prevent over-currents and trips in the VSC based STATCOM. Simulation results are presented for a 48-pulse VSC based ±100 MV AR ST ATCOM connected to a 2-bus power system. Bus voltages, and primary injected currents of STATCOM, under normal and faulted conditions shown in detail. In addition to this a nonlinear load is connected and operated at no fault conditions, and harmonics are eliminated in the source current. This enables online operation of the STATCOM and supplies required reactive power when it is most required. Thus the performance of STATCOM has improved with the new control strategy.

References

[I] N.G. Hingorani, "Power Electronics in Electric Utilities: Role Of Power Electronics In Future Power Systems," Proceedings ofthe IEEE, vol. 76, pp. 481, 1988.

[2] N.G. Hingorani and L.Gyugyi, "Understanding FACTS: concepts And Technology of Flexible AC Transmission Systems:IEEE press, 2000.

[3] L.Gyugyi, "Reactive Power Generation And Control ByThyristor Circuits," IEEE Trans. Ind. Appl., vol. la-15, no. 5, pp.521-532, Sept.ioct., 1979

[4] L.Gyugyi, "Dynamic Compensation of Ac Transmission Linesby Solid-State Synchronous Voltage Sources," IEEE, PES SummerPower Meeting, Paper No. 93 SM 434-1 PWRD, 1993.

[5] C.W. Edwards et aI., "Advanced Static Var GeneratorEmploying GTO Thyristors," IEEE, PES winter Power Meeting,Paper No. 38wml09-1, 1988.
[6] L.Gyugyi, "Dynamic Compensation of Ac Transmission Linesby Solid-State Synchronous Voltage Sources," IEEE, PES SummerPower Meeting, Paper No. 93 sm 434-1 pwrd, 1993
[7] C. Schauder et al. "TVA STATCON project: design,installation and Commissioning," CIGRE paper 14-106, 1996.
[8] E.Larsen et al. "Benefits of GTO-Based Compensation Systemsfor Electric Utility Applications," IEEE, PES summer powermeeting, Paper no. 91 sm 397-0 TWRD, 1991.
[9] J.B.Ekanayake and M.Jenkins, "A Three-Level AdvancedStatic Var Compensator," Power Delivery, IEEE Transactions on,vol. 11, pp. 540, 1996.
[10] "Evaluation of Advanced Static Var Generators," EPRIReport No. EI- 3397 MAY 1984.
[11] C. Schauder et aI., "Development of A ±100 Mvar StaticCondenser For Voltage Control Of Transmission Systems," IEEE,PES Summer Power Meeting, Paper No. 94 sm 479-6 pwrd, 1994.
[12] N.G. Hingorani et al. "Static Condenser – PrototypeApplication," CIGRE Paper, New Zealand, 1993.
[13] S.BhattachaIya, Z. Xi, " A Practical Operation Strategyfor STATCOM Under Single Line To Ground Faults In PowerSystem" ,IEEE PSCE conf.,Nov.2006,Atlanta.

IOSR Journal of Electrical and Electronics Engineering (IOSR-JEEE)
ISSN: 2278-1676Volume 3, Issue 3 (Nov. - Dce. 2012), PP 08-19
www.iosrjournals.org

Design Analysis of a 1.5kva Hybrid Power Supply for Power Reliability

[1]Ekpenyong, E.E, [2]Bam, M.E and [3]Anyasi, F.I
[1,2,]Department of Electrical/Electronic Engineering, Cross River University of Technology, P.M.B 1123, Calabar. Nigeria.
[3]Department of Electrical and Electronics Engineering, Ambrose Alli University, P.M.B 14, Ekpoma, Edo State, Nigeria.

Abstract: *Interest involves a careful design of 1.5KVA hybrid power supply for power reliability. A renewable single source system for a higher power demand application is often high in cost due to sizing of the source of supply component to meat reliability requirements.*

The system design is considered for the administrative office of the head of department, electrical and electronics engineering in Cross River University of technology, Calabar, Nigeria.

The system operate at minimum running cost, population free environment, noiseless, reliable and provide the convenient of a twenty-four hour power supply. With this system, energy efficiency is achieved by lowering demand using demand response, incorporating temporary and permanent load shifting by back-up and parallel mode respectively.

Keywords: *Hybrid power supply, Power reliability, PV system, Inverter.*

I. Introduction

Power supply from the national grid is inefficient and unreliable, hence the need to provide alternative source of power, [1]. Electrical power supply from renewable sources is advantageous as the increasing Electrical demand is a scientific contribution to the peak demand on the grid. As individuals and companies generate their power through renewable energy, the stress on the grid is reduced. However, there is an ongoing interest in the possibility of making wider use of renewable energy, particularly in homes, offices and industries, for the purpose of lighting, heating and powering of appliances. In most rural and sub-urban regions in Nigeria, inhabitants do not have access to electricity supply. Where the Electrical energy is available, it is not reliable; hence inhabitants resort to other forms of energy such as wood, paraffin, and diesel generators, which pollute the environment and cause harm to man and plants [2].

Nigeria is endowed with abundant renewable energy resources, like biomass, wind, small and large scale hydro with potential for hydrogen fuel, geothermal and ocean energies. Except for the large scale hydropower generating station which serves as a major source of electricity, the current state of exploitation and utilization of renewable energy resources in the country is very low[3]. The main constraint in the rapid development and diffusion of technology for the exploitation and utilization of renewable energy resources in the country is the absence of appropriate policy, regulatory and institutional framework to stimulate demand and attract investors. The comparative low quality of the systems developed and the high initial upfront also constitute barriers to the development of these systems.

The transmission network (that is from national grid) is overloaded with a wheeling capacity less than 4000MW. It has a poor voltage profile in most parts of the network, inadequate dispatch and control infrastructure, radial and fragile grid network, frequent system collapse, exceedingly high transmission losses [4]. It is a known fact that, Electric power availability enhances economic development of any society, while non availability of power or power outage creates economic hardship. The power sector is unable to match supply with demand of electric power and access to Electricity is low as about 60% of the population (approximately 80 million people in Nigeria) are not served with Electricity [5]. Electric power sustains the society in almost all ramifications; it becomes necessary for the Nigerian Government to sustain Electric power availability to its citizenry. Electricity has never been adequate to the Nigerian populace, for 115 years now, epileptic power supply and blackout is a regular phenomenon.

Solar energy is the energy transmitted from the sun in the form of electromagnetic radiation, which requires no medium for transmission. Solar energy is the most promising of the renewable energy sources in Nigeria, in view of its apparent unlimited potential. The sun radiates its energy at the rate of about 3.8×10^{23}KW per second. Most of this energy is transmitted as electromagnetic radiation which comes to about $1.5KW/M^2$ at the boundary of the atmosphere. After traversing the atmosphere, a square metric of the earth's surface can receive as much as 1KW of solar power, averaging to about 0.5 over all hours of daylight. Studies relevant to the availability of the solar energy resources in Nigeria have indicated its viability for practical use. Nigeria

receives 5.08×10^{12}KWh of energy per day from the sun and if solar energy appliances with 5% efficiency are used to cover only 1% of the country's surface area then 2.54×10^{6}MWh of electrical energy can be obtained from solar energy. The most common method of doing this is by the silicon solar cells. The amount of sunlight that strikes the earth in one minute could supply the world's energy needs for an entire year. The solar resource is so massive that it dwarfs every other resource on the planet. Grid-connected solar electric systems generate electricity that can be used throughout a home, business or office, thereby, reducing the amount of electricity needed to be purchase from the utility power company. When Photovoltaic power system generates more electricity than needed for use, the excess is fed back into the electric grid and a credit is received from the utility as the measuring meter reads backwards [6].

This work becomes necessary to demonstrate a Grid-connected solar power system for autonomous generation of electric power showing its efficiency, low running cost, reliability, silent operation, pollution free, minimal maintenance cost, automatic change-over system and an efficient payback system from the inexhaustible and free supply of the sun. The optimization of the system is based on numerical analytical modelling and the HOMER software package.

The quantity or amount of energy received from the sun depends on the positioning of the solar panel. Typically, the solar modules are mounted on the roof of a building but our decision for mounting this project's solar module on a stand-alone rack is to give room for further expansion as well as the renovation of the workshop without the interruption of proper functioning of the system. A very important consideration is how much sun the panel gets in the location chosen [6]. Solar cells loss efficiency in shaded locations, so the location for mounting our module was where it gets full sunlight for most hours of the day. The panels were oriented to the south-east to receive the maximum amount of sun [7]. The degree of tilt depends on the latitude at which they are installed. Panels installed at 0 to 15 degrees latitude normally have a 15 degree tilt; panels installed at 15 to 25 degrees latitude should have a tilt that is the same as the latitude. For each additional five degrees of latitude up to 40 degrees, an extra 5 degrees of tilt to the latitude is added. At latitudes of 40 degrees and above, 20 degrees of tilt is added latitude [8].

Solar power system captures the sun's energy with the help of photovoltaic (PV) cells in the solar modules. These cells are connected together side by side in flat panels or modules mounted on a roof or open area facing towards the sun. Energy from sunlight striking the top layer of the PV cells causes the cells to release electrons. These electrons migrate through the electrical system and back to the cells again, causing a DC electric current in the system, the same type of current produced by a battery. A device called an inverter converts the current from DC to AC to match the kind of current running through a standard electric outlet [9].
On cloudy days or when there is no sunshine, solar power system still produces electricity, although in lesser quantity, on this note, electricity is drawn from the battery bank to meet the energy needs in times of bad weather.

II. Materials And Method

PV Systems

Photovoltaic systems vary in complexity and depend basically on the total load demand and the availability of sunlight. The estimation here is based on hybrid principles rather than stand-alone. The major components in this system are; PV array, charge controller, inverter, battery bank, utility feeder and installation accessories. See Figure 1.

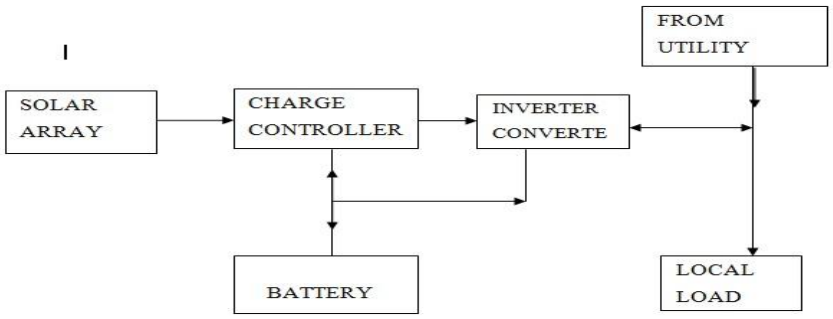

Figure1: Basic photovoltaic system integrated with grid

Source: Non- Conventional Energy Source (G.D. Rai) 2008

III. Pv Cell Arrangements

PV cells are connected in parallel to achieve the desired current and in parallel to achieve the desired voltage. The optimum operating voltage of a photovoltaic cell is generally about 0.45V at normal temperatures, and the current in full sunlight may be taken to be $270A/m^2$ [9]. A decrease or increase in the solar radiation has little effect on the voltage, but the current and power are decreased or increased proportionately. By combining a

number of solar cells in series, the voltage is increased but the current is unchanged. However, to increase the current output at the same time, several strings would be connected in parallel as depicted in the Figure 2. Consequently, if a single cell in a string should fail, the whole string would become inoperative. The cells in the remaining strings would maintain the voltage, but the current and power output of the system would be decreased by the loss of one string of cells. A short circuit in a cell would not disable the string, although there would be a slight drop in voltage. This danger could be eliminated by including a diode, which permits current flow in one direction only, at the end of each string. Alternatively, rather than have a number of strings of cells in parallel, the current and power could be increased by locating a single string of cells at the focal line of a sun tracking, parabolic trough, concentrating collector. These results in decrease in voltage because of the inevitable higher temperature of the solar cells material, but the current would increase approximately in proportion to the concentration factor of the collector [9].

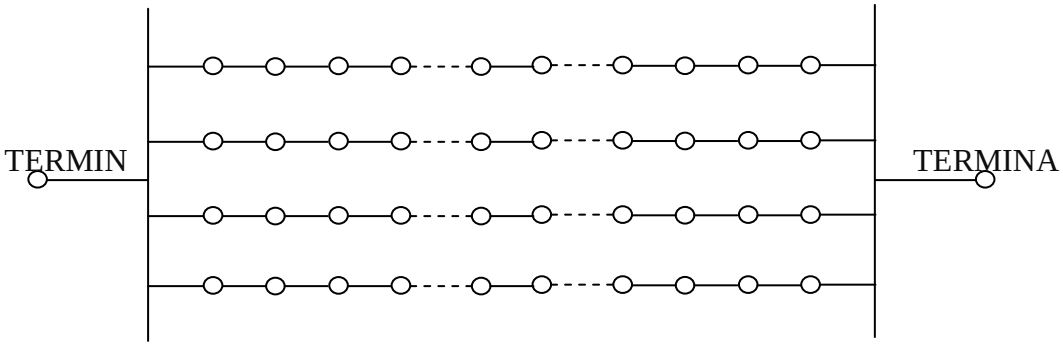

Figure.2: PV cell arrangement in series and parallel

Source: Non- Conventional Energy Source (G.D. Rai) 2008

Stand-alone PV systems: An off grid stand alone solar PV system is independent of the utility grid. Electricity from a stand-alone system is only used at the site of installation. The generated power stored in batteries is used as needed. A typical off grid house using a solar PV system is usually rated at 3 kilowatt (KW) is 15 – Kwh/day and provides power only for essential devices [10]. An off grid or stand alone PV system is independent on the commercial utility power, Electricity from an off grid system is only used at the installation. The generated power is stored in battery and used as needed. The advantage of an off grid system have freedom from the commercial utility system and in the long run lower electrical cost.These disadvantages are limitations on power consumption which is dependent on the capacity of the battery bank to supply electrical power during bad weather days and being self sufficient on power.

Loads: Most common loads are 12V, 24V, 36V, 48V, DC appliances or 220V AC appliances. The estimated power consumption is given in intervals of hours or minutes, for the length of a week, month or year. If both a DC and AC system bus exist, some of the DC bus energy can be routed through the inverter to the AC loads. The loads can posses' different priorities in terms of when they need to be met by the electricity supplied. There are optional loads which can either be supplied at the specified time instant but do not have to, and then they are suitable as dump loads. There are deferrable loads, which do not have to be supplied at the specified time instant, but need to be covered within a certain time interval. Other high priority loads need to be run at the given time instant. These loads include 5 fluorescent points, 2 ceiling fans, 5 laptops, two 14" television and 1 satellite decoder [11].

Table 1 shows a typical appliances power rating, why Table 2 shows the load estimate.

Table 1: Typical Appliances Power Rating

APPLIANCE NAME	POWER (WATTS)
Air conditioner	1350
Ceiling fan	75
Desktop computer	360
Food mixer or blender	110
Heater	1500
Iron	1100
Lighting kitchen	250
Lighting out-door	150
Lighting office	150
Microwave	1450

Radio-stereo	110
Oven	5000
Refrigerator (frost-free)	445
Toaster	1100
Vacuum cleaner	700
Water heater (electric)	3200
Television	200
Deep freezer	500
Laptop	75
Printer	100
Satellite dish	30
VCR	40
Kettle	2500
Mobile phone charger	15
Fluorescent lamp	40

Table 2: Load estimate.

S/N	APPLIANCE	QUANTITY	POWER RATING (W)	HOURLY USE (h)	TOTAL POWER (W)	ENERGY (W)
1	FLOURESCENT LAMP	5	40	6	200	1200
2	FANS	2	100	6	200	1200
3	LAPTOPS	5	65	6	325	1950
4	14" TELEVISION	2	62	6	124	744
5	SATELLITE DECODER	1	100	6	100	600
6	SPARE				250	250
					1199	**5944**

Total power becomes 1199watts
Total power in KVA becomes 1199 /0.8
= 1.498KVA
=1.5KVA. This matches with the inverter size.
Energy in watt-hour =5944Wh
Energy in kilowatt/hour = 5.9Kh

IV. PV System Design (PV Sizing)

Due to the variable nature of the energy source, one of the most expensive aspects of a PV power system is the necessity to build system autonomy to provide reliable power during periods of adverse weather or increased demands. This is accomplished by over-sizing the PV array and enlarging the battery storage, which are the two most costly system components. Improved system usage and operation may be more easily achieved with a hybrid system than with a single-source application [12]. Hybridising a PV system often reduces the need for over-sizing the PV array to achieve system autonomy especially when complementarily different energy sources can be used effectively. Photovoltaic systems here are combined with battery bank and utility supply to cope with higher energy demands or in weather by extended periods of little sunshine to form the hybrid systems. The PV sizing variables to be optimized are the size of a PV panel and the number of strings in a PV array. A photovoltaic module model based on the electrical characteristics provided by the manufacturer is considered. The model calculates the power produced by a solar module using the photo conversion efficiency formulas as shown in Equations below [12].

$$\eta = P_{STC} / E_{IN} \quad \ldots . (1)$$

$$P_{out} = \eta \cdot E_i \cdot C_f \quad \ldots (2)$$

Where:

η = Photo conversion efficiency

P_{STC} = Power at $25^{\circ}C$ and $1000W/m^2$

E_{iN} = $1000W/m^2$ Standard Test Condition (STC)

P_{out} = Power Output

E_i = Effective solar irradiation impinging the cell in W/m^2

C_f = Correction factor for η

This method is quicker and only needs the power produced by the PV module at 1000 W/m² and the irradiance level reaching the module. The method assumes that the efficiency of the solar module is constant at any irradiance level global solar radiation of Calabar (Latitude 4.97^0N, longitude 88.35^0E and altitude 6.14m above sea level) [13]. Global solar radiation data measured in $KWHm^{-2}day^{-1}$ can be converted to $MJm^{-2}day^{-1}$ using a conversion factor of factor of 3.6 [14].

Figure 3: Map of the Project Area.

Source: BritanniaEncyclopaedia

In this work, the aim isto calculatingthe number of modules needed to supply a load of 1.5KW in the H.O.D's office, Department of Electrical and Electronic Engineering, Cross River University of Technology in the city of Calabar. The solar radiation during the month of January in Calabar is 14.1300 $MJ^{-2}m^2$[32] and average sunlight hours of 4 hours [13]. The map of studied area is shown in Figure 3.

The solar radiation per hour considering 4 hours is (14.1300 $MJ^{-2}m^2$) / (4h) = 981.25W/m² per hour.

Using equation (1), the number of solar modules needed by the system using quick method can be calculated [4].

Photo conversion efficiency is calculated by

$$\eta = \frac{P_{STC}}{E_{iN}} = \frac{(110)}{(1000)} = 0.11$$

Now using equation (2), Power can be calculated thus;

$$P_{out} = \eta \cdot E_i \cdot C_f$$

= (0.11)*(981.25)*(0.95)

= 102.5W.

Now, to calculate the number of solar modules needed for the system using the quick method, we take the load power of 1498W and divide it by the power generated from the solar module (1500W)/(102.5) = 14.6.

Meaning, 15 PV module Pss 12110 simba solar module which is equivalent to 1,650watts PV is adequate to generate enough power to supply this load of 1.498 (1.5KVA) [13].

V. Batteries In A Hybrid System

Typically, battery efficiency is 80% requiring a battery bank capacity greater than what is actually needed [7]. Batteries periodically need servicing and have the highest potential offaults in a solar PV system. The important specifications to consider for selecting a battery are:
Capacity 6V dc, 350 Amp hour, 350 Amp/hour 20 hour Rate and 460 Amp/hour 100 hour rate.
Some basic steps to ensure good condition of your battery would be:

- Fully charge your battery before use.
- Be sure to fully tighten the connectors and properly wire the cables.
- Fasten vent caps tightly and check from time to time.
- Batteries should be wiped free of all corrosion, dust, and dirt frequently.

VI. Modelling Of The Battery Bank

The system batteries are connected in parallel. Positive terminals are connected to positive terminals and negative terminals to negative terminals. Parallel connections are established by mutually linking the "free" positive terminals of the "series rows" on one side, and mutually linking the "free" negative terminals on the other side [15]. The number of rows to be linked in parallel depends on the number of parallel connections to be Established by the connections. See Figure 4.

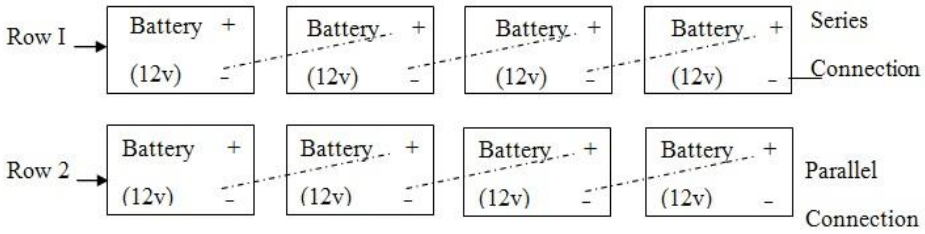

Figure 4: Parallel Connection

One set of wires – positive and negative – is connected to the charge controller (incoming current), and one set to the inverter (outgoing current) [15].The positive wires (incoming and outgoing) and the negative wire (incoming and outgoing) are best connected to diagonally opposite corners in order to equalize the charge/discharge level of the batteries (which will positively affect the sun times and battery life). The model produces a high current capacity as compared to a unit battery which is 12V, 200Ah. Thus by this configuration, the system rating becomes 24V, 400Ah. See Figure 5.

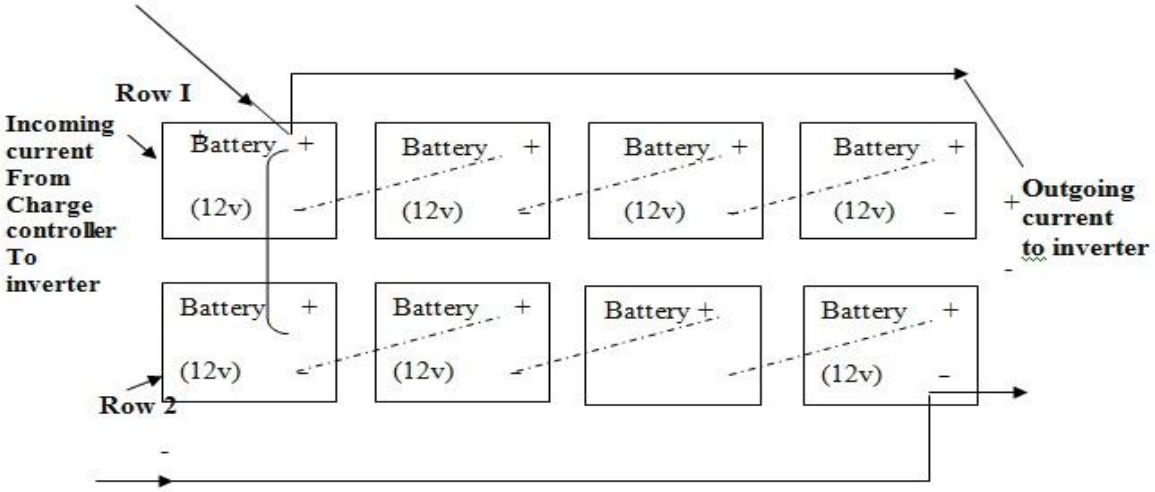

Figure .5: *Showing Incoming and outgoing current*

VII. Battery Sizing

Battery sizing consists in calculating the number of batteries needed for a renewable energy system. This mainly depends on the days of autonomy desired. Days of autonomy are the number of days a battery system will supply a given load without being recharged by a PV array, utility supply or another source. If the load being supplied is not critical then 2 to 3 autonomy days are commonly used. For critical loads 5 days of autonomy are recommended [16]. A critical load is a load that must be used all the time. The battery's capacity will decrease at lower temperatures and increase at higher temperature. The battery's life increases at lower

temperature and decreases at higher temperature. It is recommended to keep the battery's storage system at 25 ºC. At 25 ºC the derate factor is one [11].

The following procedure shows how to calculate the number of batteries needed for a hybrid energy system. Equation (3) shows how to calculate the required battery bank capacity for a hybrid renewable energy system [16].

$$B_R = \frac{L_{Ah/Day} \cdot D_{ST}}{M_{DD} \cdot D_f} \quad \ldots (3)$$

Where $L_{Ah/Day}$ is the Amp-hour consumed by the load in a day (Ah/Day)

D_{ST} is the number of autonomy days

M_{DD} is the maximum depth of discharge

D_f is the derate factor

B_R the required battery bank capacity in (Ah).

Equation (4) presents how to calculate the number of batteries to be connected in parallel to reach the Amp hours required by the system.

$$B_P = \frac{B_R}{B_C} \quad \ldots (4)$$

Where B_R is the required battery bank capacity in (Ah).

B_C is the capacity of the selected battery in (Ah)

B_P is the number of batteries that needs to be in parallel.

Equation (5) presents how to calculate the number of batteries to be connected in series to reach the voltage required by the system.

$$B_S = \frac{V_N}{V_B} \quad \ldots (5)$$

Where V_N is the DC system voltage (Volt)

V_B is the battery voltage (Volt)

B_S is the number of battery that needs to be in series.

The total number of batteries needed is obtained by multiplying the total number of batteries in series and the total number of batteries in parallel as shown in equation (6).

$$N_B = B_S \cdot B_P \quad \ldots (.6)$$

Where,

B_S is the number of batteries in Series.

B_P is the number of batteries in parallel.

N_B is the total number of batteries needed.

In this work, we sized a battery system that will supply 1498W per day to a AC electrical load. The DC voltage of the battery system will be 24V. The number of autonomy days will be 4 days. The maximum depth of discharge will be 50%. The batteries are kept at a temperature of 25ºC, thus, the derate factor is 1. We choose deep cycle Acid Battery models. It has 200Ah at 12Volts. The Amp-hour load of the system, take 1498Wh/day and divide it by 24V, is 49.9Ah/day. Then using equation (3) to (6), we calculate the batteries required by this system.

Required Battery Capacity $B_R = \frac{L_{Ah/Day} \cdot D_{ST}}{M_{DD} \cdot D_f}$

= **[(**49.9)*4]/ (0.5 *1)

= 399.2Ah

≡ 400Ah

Batteries in Parallel $B_P = \frac{B_R}{B_C}$ = [(399.2)/200] =1.99 = 2

Batteries in Series $B_S = \frac{V_N}{V_B}$ = 24/12= 2

Total Number of Batteries $N_B = B_S \cdot B_P$ = 2*2 = 4

VIII. The Inverter

An inverter is an electrical device that converts DC to AC. The converted AC could be at any required voltage and frequency with the use of appropriate transformers, switching and control circuits [11]. Inverter in this work is used to supply AC power from DC solar panels and batteries. The Grid tie inverter can feed energy back into the distribution network because it produce alternating current with the same wave shape and frequency as supplied by the distribution system and can also turn on the hybrid system automatically in the case when utility supply switches off.The electrical inverter is a high-power electronic oscillator. It is so named because early mechanical AC to DC converters was made to work in reverse, and thus was "inverted", to convert DC to AC.The inverter performs the opposite function of a rectifier. The electricity can then be used to operate AC equipment like the ones that are plugged in to most house hold electrical outlets. The normal output AC waveform of an inverter is a sine wave with a frequency of 60Hz. The efficiency of converting the direct current to alternative current of most inverters today is 90 percent or more. Many inverters claim to have higher efficiencies but for this project the efficiency used is 90%. [9] The inverter has output voltage of 220V and produces a sine wave AC output signal of 60Hz [17].

A Sine wave inverter produces voltage with low total harmonic distortion (normally below 3%). It is the most expensive type, which is used when there is a need for clean sinusoidal output for some sensitive devices such as medical equipment, laser printers, stereo, etc. sine wave inverters put out a wave that is the same as that you get from the power company. Often times it is even better and cleaner. Sine wav inverters can run anything, but are also more expensive than other types. One solution to the problem of a few small appliance not working well with modified sine wave inverters is to get a large wattage of modify inverter. This gives more tolerance, and allows it to give better efficiency powered up without having to run the larger inverter to full capacity. This is the advantage of pure sine wave inverter over other type of inverters.

There are a number of topologies used in the power inverter circuits. Cheap square wave circuits suitably primarily for this kind of work may also use a push-pull converter with a step-up transformer. Most commercially manufactured models use the same basic multi-stage concept; first a switching pre-regulator (SMPS) steps up a voltage from an input source to a DC voltage corresponding to the peak value of the desired AC voltage. The output stage generates an AC. This stage usually uses a full-bridge configuration. If a half bridge is used, the DC-link voltage should be at least twice the peak of the generated output voltage. Input to output galvanic isolation is provided by either a high-frequency transformer in the SMPS switching pre-regulator, or by a large low-frequency output transformer [8]. If a low-frequency transformer is used, the sinusoidal voltage is generated on its primary side and transformed to the secondary side. The output voltage level can be controlled either in square-wave mode or in pulse width-modulated (PWM) mode. Sine wave circuits use PWM mode, in which the output voltage and frequency are controlled by varying the duty cycle of the high frequency pulses. Chopped signal then passes through a low pass LC-filter to supply a clean sinusoidal output. [18]. See Figure 6.

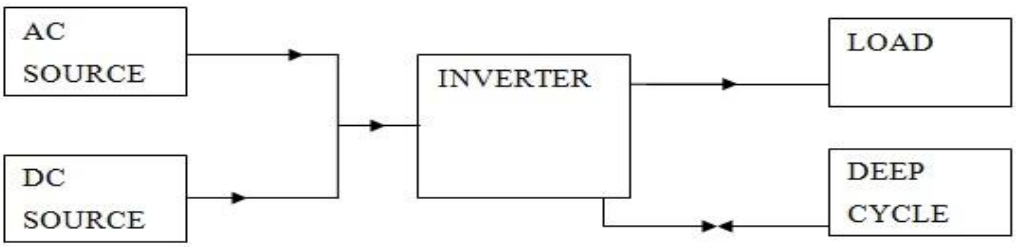

Figure 6: Block diagram of an inverter system

Analytical Method

This method can be used to select the correct size of the resistor that is suitable to produce 50Hz frequency. Using the formula,

F = 0.22/RC

Where,

F = 50Hz (PHCN)

C = 0.1×10^{-6} F

50 = $(0.22 \times 10^{-6}$ F)/ $0.1 \times$ R

5R = 0.22×10^{-6}

$R = (0.22 \times 10^{-6})/ 5$
$R = 44000$
$R = 44K\Omega$
Hence sending switching with variable resistor size of 50KΩ and 0.1×10^{-6} F capacitor, frequency switching of 50Hz is guaranteed [19].

Operation of 1.5KVA (24/220V) single phase inverter

When the switch S_1 is switched ON, the current is passed from 400Ah deep cycle battery of 24V to the voltage regulator and the regulator 7805IC generate 5V to the oscillator IC4047, this oscillator is an astablemultivibrator which gives out the square wave – signal at pin 10 and 11 [20]. This oscillation is adjusted to frequency of 50Hz using the expression F = 0.22/RC, by vibration of 50KΩ variable resistor about 46KΩ, the oscillation of 50Hz is released to trigger the base current to flow to the transistor (PREAMP), the transistor switches at this frequency when there is base current that is limited by 100Ω resistor, this signal from emitter terminal of the transistor is amplified and drive the gate of MOSFET(IRFZ150)which switches the 24V in secondary winding of centre tap transformer at 50Hz frequency and the output voltage is 220V at primary of the transformer which depend on turn ratio of transformer $V_1/V_2 = N_1/N_2$.[20]. See Figure 7 for the complete diagram of the 1.5KVA inverter system.

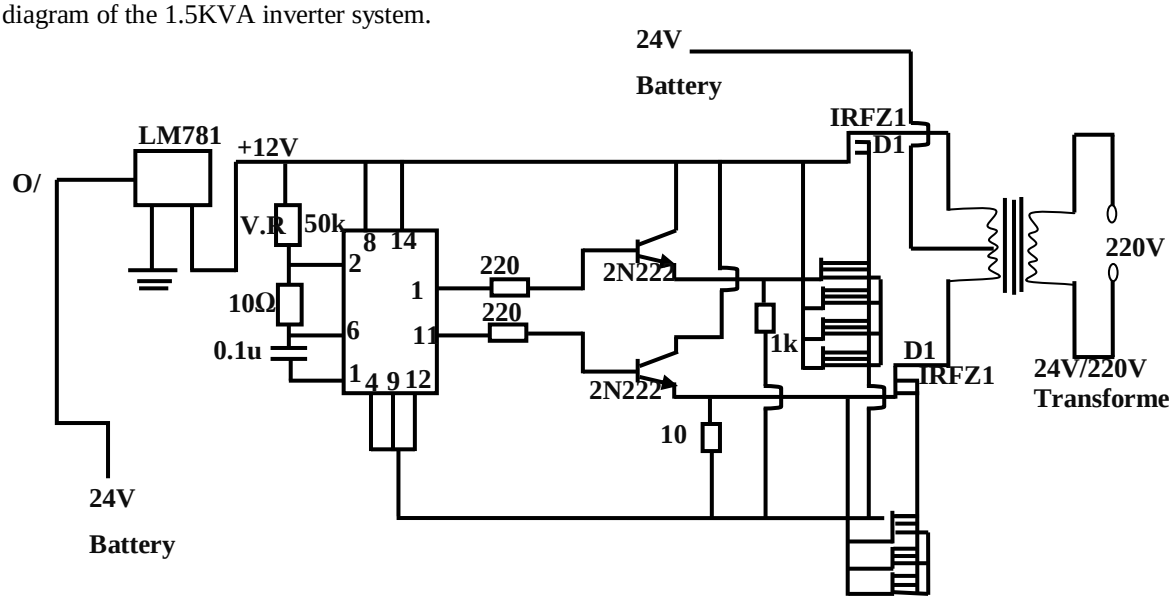

Figure 7: Circuit diagram of 1.5KVA inverter using IC CD4047 +IRFZ150

The inverter system gives out an output of steady AC voltage which makes it suitable to be used in powering sensitive electronics (equipment) like the ones used in this project. This inverter uses 3 – stage chargers, so it can be left powered up all the time because of the inbuilt power relay. Meaning that, when running from AC, the power feeds through an inverter, at the same time, some power is being tapped for the battery charger. If the AC power goes out, the inverter automatically switches to battery power. In most cases it is difficult to notice it but for a light flicker, it is so fast because of the two transistor analogy of a thyristor which is part of the circuit. This system is designed to work automatically, it does not require anyone to be employed to physically turn it ON/OFF before it can charge the battery and at the same time, when required; supplies current to the appliances.

Inverter Design

The solar inverter is a critical component of an entire solar energy system. It performs the conversion of the variable DC output of the PV cells into a clean sinusoidal 50Hz [11] current suitable for supplying the commercial electrical grid or local electrical network.Inverters are usually sized according to the maximum required continuous power output. Most inverters are capable of handling three to six times more power than their rated size for short periods of time in order to accommodate surge currents which occur when starting a motor.An inverter needs to be sized to cover peak or non-surge peak load [11].

Sizing of the inverter in hybrid power supply system

Inverter sizing consists in calculating the number of inverters needed for the PV system. In small hybrid systems such as these, one inverter is enough to supply the power but for a larger hybrid system more

inverters may be needed. When you select an inverter you must have a DC voltage equal to your inverter DC voltage and have an AC voltage and frequency equal to your home and utility values [12].
Equation (7) shows how to calculate the number of inverters needed for a stand- alone hybrid system [12].

$$\text{Number of Inverters required} = \frac{P_{LOAD}}{P_{INVERTER}} \quad \ldots (7)$$

Where P_{LOAD} represent the maximum continues power load your System consumes. $P_{INVERTER}$ is the maximum power that can be supplied by the inverter.
In this project, the number of inverters needed for the energy system that have an AC load of 1498W is calculated. We have to select an inverter with an output power of 1199W or more. The inverter model used has an output of 1500W at 220V. Using equation (7): [12]

$$\text{Number of Inverters required} = \frac{P_{LOAD}}{P_{INVERTER}} = 1498/1500 = 0.99 = 1$$

The total number of inverters needed is one.

Over Voltage Regulator

The overall operation of the voltage regulator will be discussed as follows.

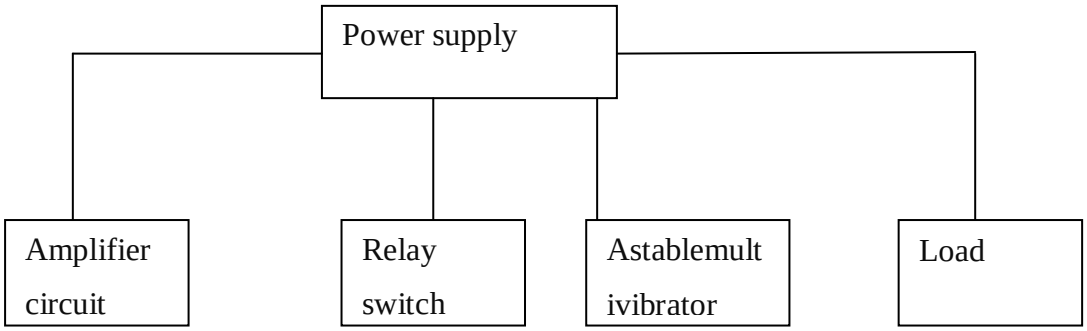

Figure 8: System's block diagram

The Power Supply Unit (PSU)

$\frac{V_{out}}{I_c} = RL$ . . . (8)

Where,
$V_{out} = 30V \text{ and } I_c = 3A$
The value of RL will then be
$V_{out} = RL\ X\ I_c$ . . . (9)

$$R = \frac{30}{3} = 10\Omega$$

Filtering Capacity Calculation

$C_f = \frac{1}{\sqrt[2]{2 \times K \times F \times Rl}}$ . . . (10)

Fr = Ripple frequency
K = Ripple factor
RL = Load Resistance
It should be noted that:
Fr = 100Hz (According to GB standard F = 50Hz × 2)
K = R. M. S. Ripple voltage/ DC output voltage
RL =20 to 100Ω
Chosen value
Fr = 100Hz
R.M.S ripple voltage = transfer current rating × RL
= 500Mv
Therefore,

$$k = 50 \times \frac{10^{-3}}{10}$$
$$= 50 \times 10^{-2}$$

$$C_f = \frac{1}{\sqrt[2]{2.100 \times 50 \times 10^{-3} \times 20}}$$
$$= 3300\mu f \ (available\ value)$$

Design Equation of an AstableMultivibrator (AMV)

$F = 1.44(R_A + 2R_B)C_t$ . . . (11)

Where,
R_A =Astable resistor
R_B = Biasing resistor
C_f =Timming capacitor
F = frequency of oscillation

IC 7805 Voltage Regulator

In the alternative, **IC 7805** can be used for voltage regulation.The IC 7805 is basically used in this project for the voltage regulation. This IC provides a fixed positive output voltage. Although, many types of IC regulators are available, the 7800 series of IC regulators is the most popular. The last two digits in the part number indicate the DC output voltage. For example, from the data table below, the 7812 is a +12V regulator whereas the 7805 is a +5V regulator. This 7800 series provides fixed regulated voltages from +5V to +24V as shown in Table 3, [20].

Table3: The 7800 seriestable

TYPE NUMBER	OUTPUT VOLTAGE
7805	+5.0V
7806	+6.0V
7808	+8.0V
7809	+9.0V
7812	+12.0V
7815	+15.0V
7818	+18.0V
7824	+24.0V

Source: V.K. Metha&RohitMetha, 'Principles of Electronics'. 2008.

Integrated circuits (IC) are preferred for voltage regulator because properties like thermal compensation, short circuit, protection and surge protection can be built into the device.

IX. Conclusion

The system designed is to be used in conjunction with the electrical system of the office facility for use during the day or day light hour and when grid power is down. It can also work the other way, when the solar PV does not produce enough electricity, it can draw power from the grid. This is done automatically through a device that monitors the available power and switches between PV and grid power. The design of hybrid system is more complicated and expensive, but they are the most effective in providing constant and reliable electricity. The grid tie inverter feed energy back into the distribution network because it produces alternating current with the same wave shape and frequency as supplied by the distribution system and can also turn on the hybrid system automatically in the case of power failure. The aim of this work was to demonstrate that Hybridization of various renewable energy sources and battery bank is a key for system cost effectiveness and high performance than any other variant based on a single renewable source. The sizing results suggests that HOMER softwareis a powerful, efficient and flexible tool that gives the optimum and cost effective systems based on renewable source.

References

[1] Akpama, E.J.,"Designing a photovoltaic sustained sector: a review of current practice,"domestic use of energy conference, pp 155-160. 2011.

[2] M. Marvwan& H. ImadIbrik, "Techno- economic feasibility of energy supply of remotevillages as Palestine by PV- systems, diesel generators and electric grid," renewable andsustainable energy. Reviews pp 128-138, 2006.

[3] Sambo, A.S., International centre of energy, "Energy and Development Report, Renewable Electricity Action Program," federal ministry of power and steel, Nigeria 2006.

[4] Augustine C. &Nnabuchi M. N. "Relationship between Global Radiation And Sunshine Hours ForCalabar, Port Harcourt And Enugu, Nigeria." International Journal of physical sciences vol. 4(4), pp.182-188, 2009.

[5] Chimeka I. U, &chineke T. C. "Evaluating The Global Solar Energy Potential AtUturu, Nigeria."International journal of physical sciences.Vol.4(3), pp 115-119, 2011.

[6] Dusabe, J.L. Munda, &Jimoh A.A. "Small Scale Solar Energy System in Rwanda: Status. And Sustainability."Domestic use of energy conference, pp 137-141, 2009.

[7] Rogers A. Messenger, "photovoltaic" floridaatlantic university, 2006.

[8] Retrieved from " http://en.wikipedia.org/wiki/portal:Renewableenergy."

[9] G.D. Rai, "non-conventional energy sources."Khannapublishers 2-B, Nath market, NaiSarak Delhi-m110006. India.2008.

[10] Donald E.O. & David E.C., "Utility Grid-Connected Distributed Power Systems."National solar energy conference.ASES solar, 1996.

[11] Gabrielle Seeling-Hochmuth, "Optimisation of Hybrid Energy Systems Sizing and Operation Control." 1998.

[12] Ani, V.A. &Nzeako A.N.," Energy Optimization at GSM Base Station Sites Located inRural Areas," international journal of energy optimization and engineering (IJEOE), 2011.

[13] Augustine C. &Nnabuchi M. N. "Relationship between Global Radiation And. Sunshine Hours ForCalabar, Port Harcourt And Enugu, Nigeria." International Journal of physical sciences vol. 4(4), pp.182-188, 2009.

[14] Sabbert C., &Seeling-Hochmuth G. "Review of hybrid energy system design andperformance. "EDRC, University of Cape Town, 1997.

[15] [PVDI] solar energy international."Photovoltaic Design and Installation Manual,"New Society Publishers, 2007.

[16] Patel M.,"Wind and Solar Power Systems," second edition, Taylor& FrancisGroup, 2006.

[17] Igbal M.,"An Introduction to Solar Radiation."Academy press. New York, pp. 6-51 1983.

[18] Peter Lilienthal, Tom Lambert etal, National Renewable energy laboratory."Getting Started Guide For HOMER Version 2.1". 2005.

[19] Sandia, "Stand-Alone Photovoltaic Systems." A Handbook of Recommended Design Practices.Sandia National Laboratories. 1994

[20] Paul Breeze, "Power generation technologies." 2005

[21] Semiconductor components, function IC CD4047 Datasheet, http://www.functionic cd 4047. 2012.

[22] Fairchild semiconductor, "FQP17N40Datasheet,"http://www.fairchildsemi.com/ds/fq/fqp17N40.pdf.2012

[23] V.K. Metha&Metha."Principles of electronics"s.chad technical,2007.

[24] http://www.biomassenergycentre.org.uk/portals/page.

IOSR Journal of Electrical and Electronics Engineering (IOSR-JEEE)
ISSN: 2278-1676Volume 3, Issue 3 (Nov. - Dce. 2012), PP 20-27
www.iosrjournals.org

Performance Analysis of an Installed 1.5kva Hybrid Power Supply

[1]Ekpenyong, E.E, [2]Bam, M.E and [3]Anyasi, F.I
[1,2]Department of Electrical/Electronic Engineering, Cross River University of Technology, P.M.B 1123, Calabar. Nigeria.
[3]Department of Electrical and Electronics Engineering, Ambrose Alli University, P.M.B 14, Ekpoma, Edo State, Nigeria.

Abstract: *This work models a 1.5KVA grid connected solar power supply system using a combination of PV array, charge controller, inverter, battery bank, A.C load and installation accessories which work complementarily to capture the best feature of the energy resources and provide the grid-connected location with the highest electricity network quality and reliability. The system operate at minimum running cost, population free environment, noiseless, reliable and provide the convenient of a twenty-four hour power supply. With this system, energy efficiency is achieved by lowering demand using demand response, incorporating temporary and permanent load shifting by back-up and parallel mode respectively. The system was installed at the administrative office of the head of department, electrical and electronic engineering department in Cross River University of technology, Calabar, Nigeria. The total energy is obtained by direct inspection and energy audit. The optimization of the system is based on numerical and analytical modelling and HOMER software package. The sizing results suggest that HOMER software is a powerful, efficient and flexible tool that gives the optimum and cost effective system based on renewable source.*

Keywords: *Performance analysis, Hybrid power, derating factor, HOMER's software*

I. Introduction

The increasing demand of energy, the continuous reduction of natural resources of fossil fuels and the growing concern regarding the environment pollution, determined the mankind to explore new production technologies of electrical power using non-polluting renewable sources, such as wind energy, solar energy, sea waves, biomass [1] as well as geothermal energy, bio-fuel, hydropower, tidal power etc. Electrical power supply from renewable sources is advantageous as the increasing Electrical demand is a scientific contribution to the peak demand on the grid. As individuals and companies generate their power through renewable energy, the stress on the grid is reduced. However, there is an ongoing interest in the possibility of making wider use of renewable energy, particularly in homes, offices and industries, for the purpose of lighting, heating and powering of appliances. In most rural and sub-urban regions in Nigeria, inhabitants do not have access to electricity supply. Where the Electrical energy is available, it is not reliable; hence inhabitants resort to other forms of energy such as wood, paraffin, and diesel a generators, which pollutes the environment and cause harm to man and plants [2].

Nigeria is endowed with abundant renewable energy resources, like biomass, wind, small and large scale hydro with potential for hydrogen fuel, geothermal and ocean energies. Except for the large scale hydropower generating station which serves as a major source of electricity, the current state of exploitation and utilization of renewable energy resources in the country is very low[3]. The main constraint in the rapid development and diffusion of technology for the exploitation and utilization of renewable energy resources in the country is the absence of appropriate policy, regulatory and institutional framework to stimulate demand and attract investors. The comparative low quality of the systems developed and the high initial upfront also constitute barriers to the development of these systems.

The transmission network (that is from national grid) is overloaded with a wheeling capacity less than 4000MW. It has a poor voltage profile in most parts of the network, inadequate dispatch and control infrastructure, radial and fragile grid network, frequent system collapse, exceedingly high transmission losses [4]. It is a known fact that, Electric power availability enhances economic development of any society, while non availability of power or power outage creates economic hardship. The power sector is unable to match supply with demand of electric power and access to Electricity is low as about 60% of the population (approximately 80 million people in Nigeria) are not served with Electricity [5]. Electric power sustains the society in almost all ramifications; it becomes necessary for the Nigerian Government to sustain Electric power availability to its citizenry [6]. Electricity has never been adequate to the Nigerian populace, for 115 years now, epileptic power supply and blackout is a regular phenomenon.

Solar energy is the energy transmitted from the sun in the form of electromagnetic radiation, which requires no medium for transmission. Solar energy is the most promising of the renewable energy sources in Nigeria, in view of its apparent unlimited potential. The sun radiates its energy at the rate of about 3.8×10^{23}KW per second [7]. Most of this energy is transmitted as electromagnetic radiation which comes to about 1.5KW/M^2 at the boundary of the atmosphere.

This work becomes necessary to demonstrate a Grid-connected solar power system for autonomous generation of electric power showing its efficiency, low running cost, reliability, silent operation, pollution free, minimal maintenance cost, automatic change-over system and an efficient payback system from the inexhaustible and free supply of the sun. The optimization of the system is based on numerical analytical modelling and the HOMER software package.

Typically, the solar modules are mounted on the roof of a building but our decision for mounting this project's solar module on a stand-alone rack is to give room for further expansion as well as the renovation of the workshop without the interruption of proper functioning of the system. A very important consideration is how much sun the panel gets in the location chosen.

II. Materials And Method

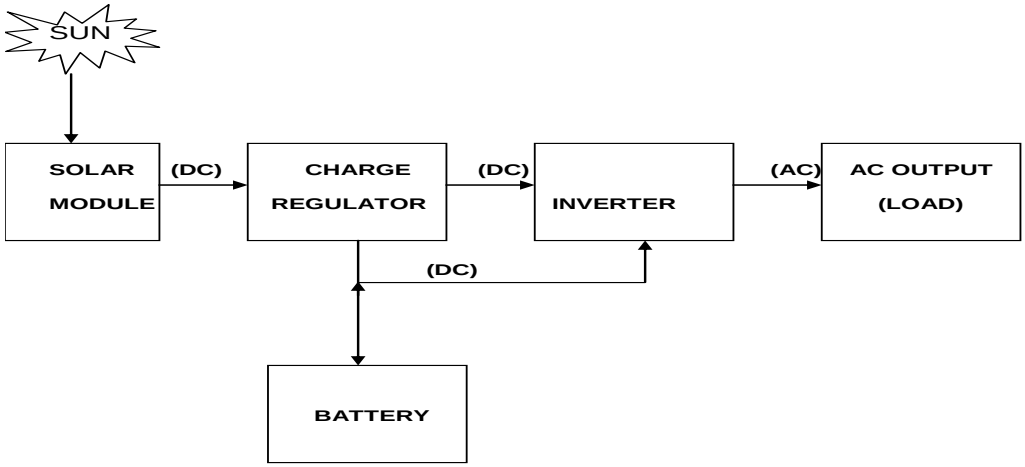

Figure1: block diagram of the solar energy system

PV Installation: PV arrays for PV system are installed in many unique and innovative ways. However, there are common issues involved in any installation, whether the array is fixed or tracking, mounted at ground level or on a pole or on the roof of a building [8]. PV arrays are mounted at a fixed angle of 45 degrees facing east or on a tracking device that follows the sun, allowing them to capture the most of the day. The objective is to solidly mount PV array that will last for many years and withstand all kinds of weather. Customized array mounting structures are excluded in this project because of cost [9].

In general, roof mounting of PV modules is more complex than pole mounting. Roof mounts are more difficult to maintain, particularly if the roof orientation and angle are not compatible with the optimum solar tilt angle. If a roof mount is required, it is good practice to allow a clear space between roof and the array. The array will operate cooler and produce more energy if it stands off the roof at least 3 inches [9]. Flushing mounting PV modules to the roof of a building is not recommended as the modules become more difficult to test and replace, and the performance of the array is decreased because of the higher operating temperatures.

System Wiring: Wiring is used to distribute power to various devices selecting the correct size and type of wire enhances performance and reliability of solar PV system. The size of wire must be large enough to carry the maximum current without causing any voltage losses. When wiring up your solar energy system, make sure all wires are properly marked. This small effort during the installation process will significantly ease trouble shooting later: it enables you to identify wires at a glance without having to open cable trunks/dig up wires to see which one is leading where, or having to do complicated tests with a multi-meter. More importantly, it prevents cables from being displaced – which may be dangerous and damaging to your equipment [9].

Installation Configuration: The installation in this work is based on hybrid on-grid systems. The system essentially uses the existing commercial utility system for power and store electricity power in a battery. A solar PV system is installed into electrical system of the office facility for use during the day or day light hour and

work when grid power is down. It also work the other way, when the solar PV does not produce enough electricity, it can draw power from the grid. If more electricity is produced than what is needed, the excess can be put back on the grid this is done automatically through a device that monitors the available power and switches between PV and grid power. A second utility meter can be added to keep track of how electricity has been put back on the grid action fee, the liability of solar component in the initial cost of the solar PV system [10].

A combination of an on grid and up grid solar PV system has the advantages of both a hybrid system is connected to the grid in case of poor weather or night use, but also has a battery bank to store electricity in case utility grid power is lost. The design and installation of hybrid system is more complicated and expensive, but they are the most effective in providing constant, reliable electricity [10].

Energy analysis: The equipments considered are photovoltaic solar modules, inverter, battery bank and loading system. The energy analysis carried out using HOMER software is shown in Figure 2.

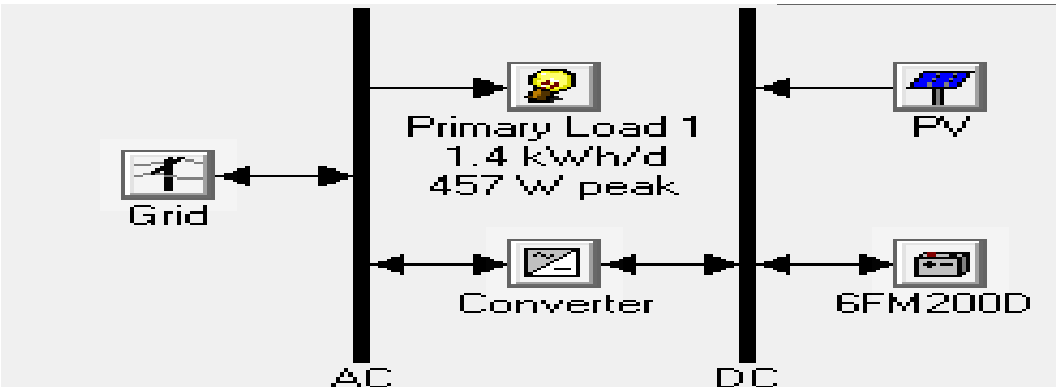

Figure 2: Homer Configuration of the system

Expected Configuration of the system: The maximum power delivered by the hybrid power system is 1.5KW, thus the DC/AC inverter has a rated power of 1.5KW to cover the power peaks;

- The DC bus is set to 24V
- The average monthly electric energy consumption of the system is 36KWh/month with a maximum delivered electric power to the system of 456W as shown in Fig 1.
- The 15 PV panels of 110Wp per unit with output voltage of 24V d.c to account for PV efficiency.
- The batteries are of vision 6FM 200D type, characterized by 12V d.c. and 200Ah; their number is multiple of 2 because the d.c bus bar voltage is 24V d.c.

Daily load profile: The load profile is based on the H.O.D's office as shown in Fig 3, Peak loads of 240W run on the system throughout six (6) hours of the working days. The total daily load average 1440watt-hours per day. The seasonal load profile is shown in Figure 4.

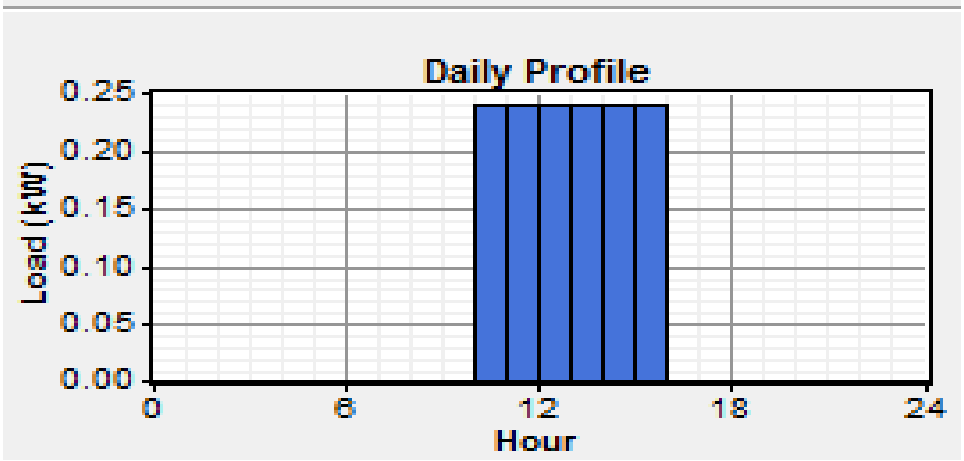

Fig 3: Daily load profile

Seasonal load profile

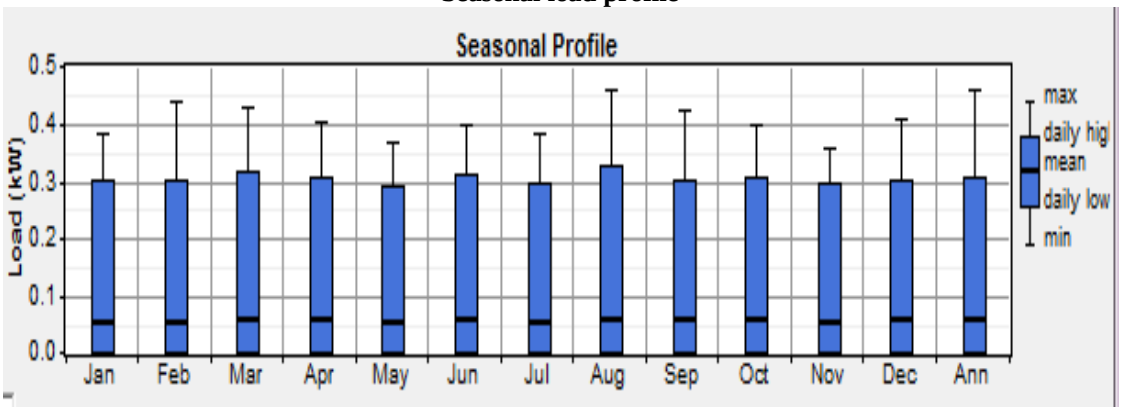

Figure 4: Seasonal load profile

Maximum power possible: The maximum power output of the installed PV is 0.2kw and is not adequate to charge the battery let alone power the 1.4KW load. This accounts for the blackout in the PV area. HOMER discards systems that do not satisfy the specific constraints so that they do not appear in the optimization or sensitivity results. However, the required PV size adequate for the installation is 1.65KW (13 more PV modules of 110W each is required to make up for this shortfall). Figure 5 shows the contribution of the PV in the installed system.

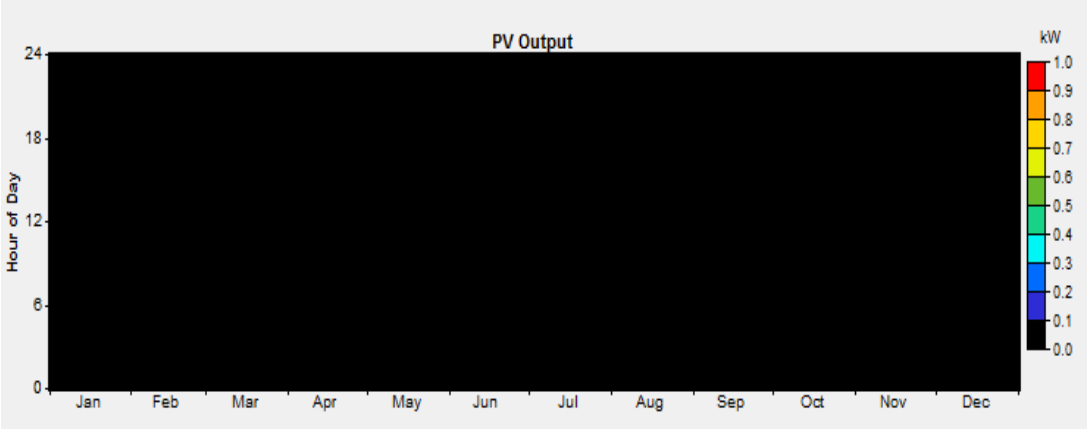

Figure 5: PV Output

Data Map (D-Map)

Data map (D-map) is a type of graph showing one year of time series data. With time of day on one axis and day of the year on the other, each time steps of the year is represented by a rectangle which is coloured according to the data value for that hour. The Dmap format often allows you to see daily and seasonal patterns more easily than you could with a simple time series plot. The D-map for the system is shown in Figure 6.

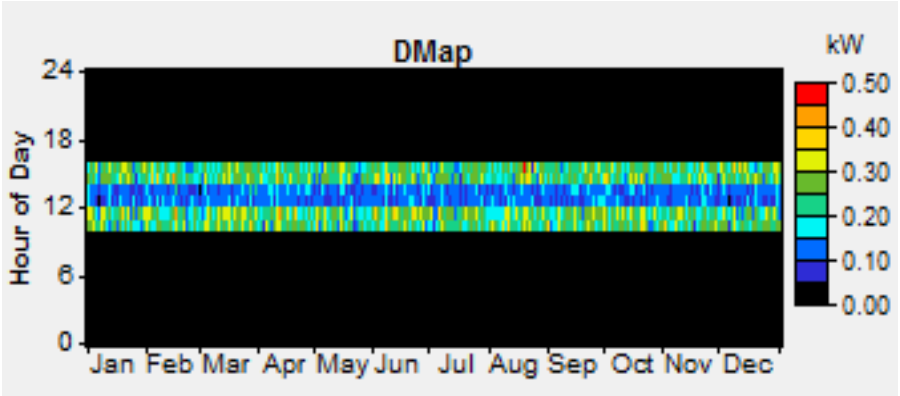

Figure 6: Data Map (D-Map)

Solar Radiation Profile: Solar radiation and clearness index data is shown in Figure 7 (a).

Location

Latitude 4 ° 950 ' North Sou

Longitude 8 ° 317 ' East We

Data source: Enter monthly averages Impo

Baseline data

Month	Clearness Index	Daily Radiation (kWh/m2/d)
January	0.540	5.133
February	0.519	5.197
March	0.460	4.788
April	0.444	4.617
May	0.423	4.260
June	0.364	3.574
July	0.330	3.266
August	0.337	3.437
September	0.332	3.433
October	0.363	3.657
November	0.435	4.169
December	0.525	4.883
Average:	0.421	4.196

Scaled annual average (kWh/m²/d) 4.2

Figure 7(a): Solar radiation and clearness index data

Figure 7 (b) shows the solar resource profile over one year. The approximate location of the site used is $4^{0}\,950^{1}$N and $8^{0}\,29^{1}$ E. The solar resource data for Calabar, Nigeria was obtained from International Journal of Physical Sciences Vol. 4 (4), pp. 182-188, April, 2009 online at http://www.academicjournals.org/IJPS [11]. The solar radiation in Calabar is highest in the months of January, February, November and December. At these periods the PV output is highest as shown in the solar radiation graph in Figure 7(b).

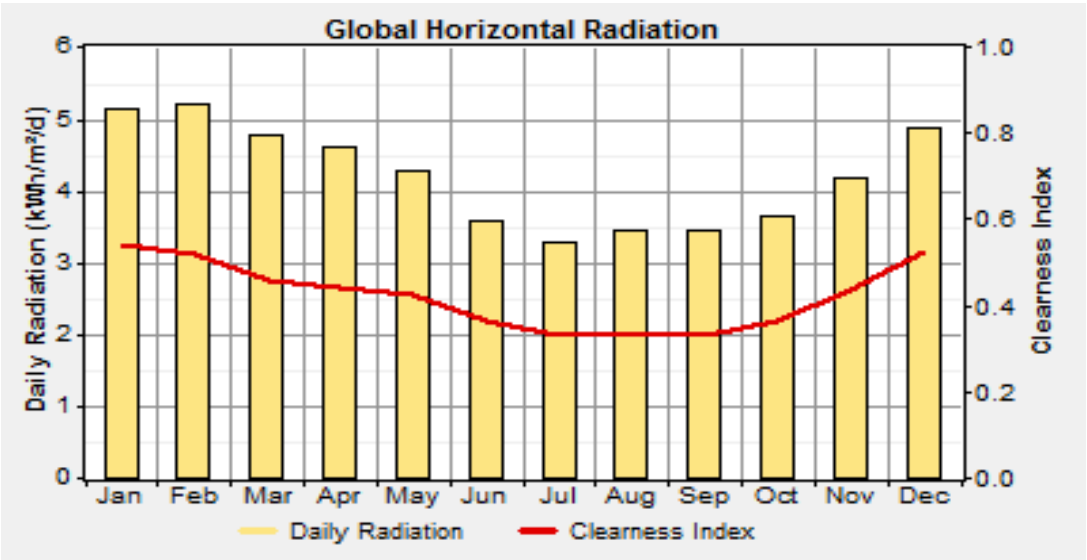

Fig 7 (b): Global Horizontal solar radiation graph

Economic Analysis: All costs associated with the Photovoltaic solar cells, including modules, mounting hardware and installation.

III. Capital And Replacement Cost Curve Of PV System

The capital and replacement costs were specified at $1000 and $800 respectively. A low maintenance cost was considered for the PV system because little or nomaintenance is needed for the panels and a derating factor of 80% and 20 years lifetime as shown in Figure 8.

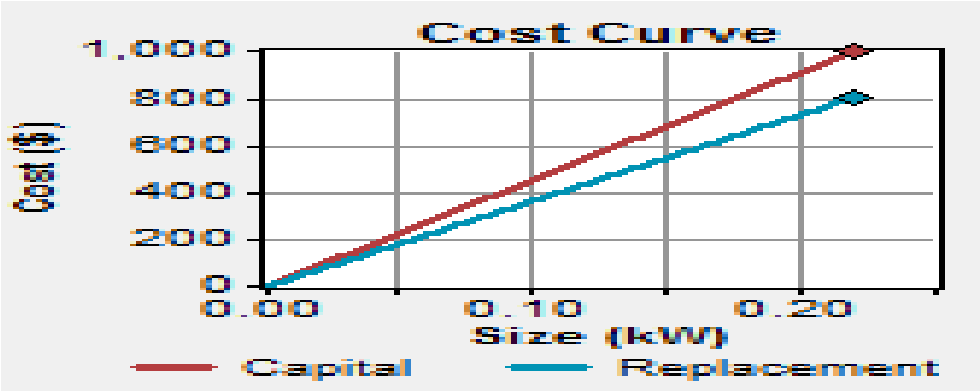

Figure 8: Capital and Replacement Cost Curve

The work life year was taken as 20 years. All calculations are done with exchange rate of N160. The tariff of the utility company in Nigeria, the power holding company of Nigeria (PHCN), is N130 per Kwh ($0.813).

Cost of Charge controller: HOMER does not model the battery charge controller as a separate component. So, its cost and efficiency is usually included in the values specified for other components. For grid-connected PV system simulations, the best place to include the charge controller costs and efficiency is the PV array inputs. Then the PV derating factor is reduced to account for the efficiency of the charge controller. Hence, the derating factor of 80%.

Battery bank cost profile: The battery bank cost profile is shown in Figure 9.

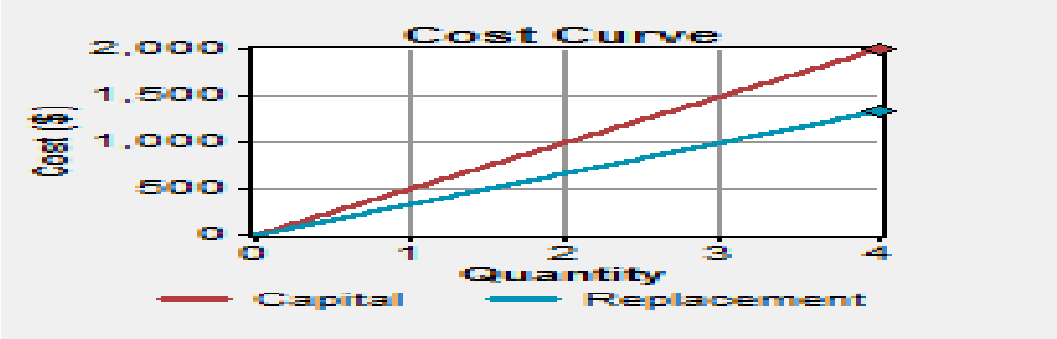

Figure 9: Battery cost graph

The capital and replacement costs were specified at $500 and $333 per battery respectively. Capital cost value of the battery include all costs associated with the battery bank, such as mounting hardware installation, labour and cost of a rack, room or building that houses the battery. The battery chosen is the 6FM200D series. It has a nominal voltage of 12 volts and nominal capacity of 200Ah/2.4kwh with 4 years lifetime. Two batteries were considered by HOMER in the simulation as shown in Figure 9.

Inverter cost profile: The inverter costs include all the costs associated with the inverter, such as hardware and labour. The factors that gave rise to the curve as shown in Figure 10 are, inverter size, capital cost, replacement cost operation and maintenance cost, lifetime of 15years and inverter efficiency of 90%.

Figure 10: Inverter cost graph

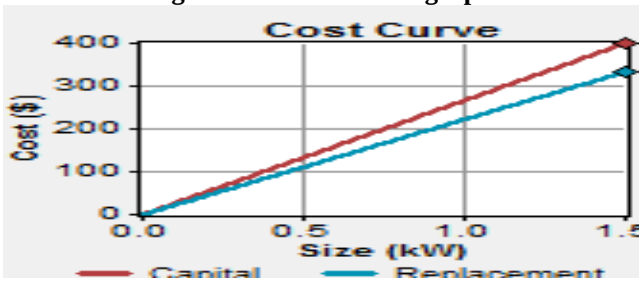

Cost summary: Table 1 shows the cost summary

Table 1: shows the cost summary

Components	Size	Capital costs($)	Replacement cost($)	O&M cost ($)	Lifetime
PV panels	0.220 (KW)	1000	800	0.50/year	20years
Battery	200Ah/12V (bank size: 4 batteries)	333/battery	333/battery	2.00/year	4years or 1000kwh of throughput per battery
Inverter	1.5KVA	400	333	1.00/year	15years

IV. Sensitivity and Optimization simulation result

HOMER's main economic output is the net present cost. All systems are ranked according to net present cost, and all other economic outputs are calculated for the purpose of finding the net present cost. The result obtained from the optimization gives the initial capital cost as $5,833 and operating cost as $260/year, total present cost (NPC) is $9,160 and cost of energy (COE) is $1,363/kwh. The payback period of the system is 25years and not 20years as specified as the manufacturers. See Figure 11.

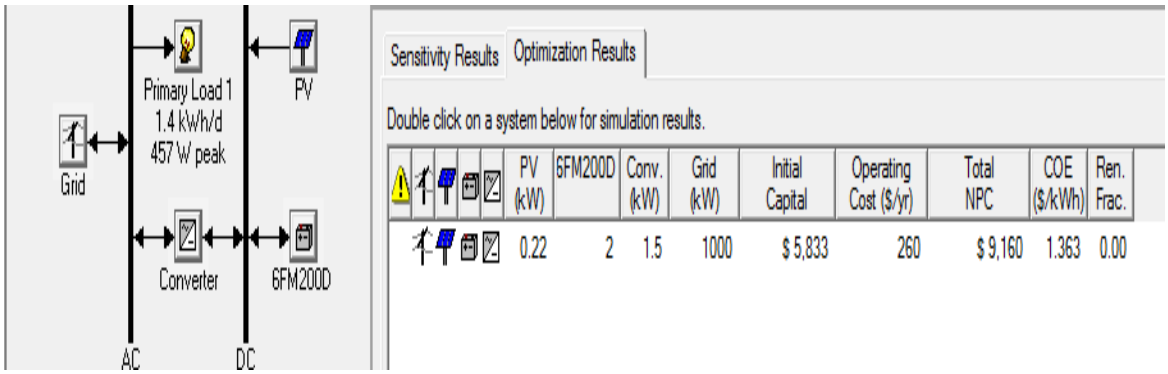

Figure 11: Sensitivity and Optimization simulation result

Load levels: The loads considered are typical domestic loads and include 5 fluorescent points, 2 ceiling fans, 5 laptops, two 14" television and 1 satellite decoder. The load input table is as shown Table 2.

Table 2:load input table (Baseline Data)

Month: January
Day Type: Weekday

HOUR	LOAD(KW)
10:00 – 11:00	0.240
11:00 – 12:00	0.240
12:00 - 13:00	0.240
13:00 – 14:00	0.240
14:00 – 15:00	0.240
15:00 -16:00	0.240

Consequently the average load per day is 1.44kwh/d, average load per hour is 0.06kw/h, and peak load is 0.457kw and load factor of 0.131 all shown in Table 3.

Table 3: load table

	BASELINE	SCALE
AVERAGE (Kwh/D)	1.44	1.44
Average (Kw)	0.0600	0.0600
Peak (Kw)	0.457	0.457
Load Factor	0.131	0.131

V. Payback period

Research has shown that the lifespan of a PV system is between 20 and 25 years. Benefits abound in the choice of solar PV for self generation of electric power. Environmentally, solar power does not contribute to greenhouse gas emission. The payback period of solar power is estimated using the simple payback method as follows;

Payback period = purchase and installation cost/ Expected annual savings.

For this project, the purchase and installation cost for the 1.5KVA PV stood at $9,160 and cost of energy from utility supply per annum $1,363.

Therefore, Payback period = $9,160 / $1,363

= 6.72years

=7years.

The payback period is estimated at about 7 years. From this fact, the cost of the PV project will be paid off within 7 years while the remaining years is on profit making.

VI. Conclusion

The installation in this work at Latitude $4^0$950'' North and longitude 8^0 317'' East is based on hybrid on-grid system. The system essentially uses the existing commercial utility and solar PV system for power and store electricity power in a battery. The system is installed into the electrical system of the office facility for use during the day or day light hour and when grid power is down. It can also work the other way, when the solar PV does not produce enough electricity, it can draw power from the grid. This is done automatically through a device that monitors the available power and switches between PV and grid power. The installation of hybrid system is more complicated and expensive, but they are the most effective in providing constant and reliable electricity. The grid tie inverter feed energy back into the distribution network because it produce alternating current with the same wave shape and frequency as supplied by the distribution system and can also turn on the hybrid system automatically in the case of power failure. The payback period is estimated at about 7 years. From this fact, the cost of PV work will be paid off within 7 years while the remaining years is on profit making. For the system to run as stand alone, the existing system should be upgraded by adding 13 more of same size of PV module and two additional 200Ah deep cycle batteries. A second utility meter can be added to keep track of how much electricity has been put back on the grid. Sun tracking parabolic trough and concentrating collectors could be added to improve the solar irradiation on the system. Provision could be made for the PV arrays to be mounted at a fixed angle of 45 degrees facing east or on a tracking device that follows the sun, allowing them to capture the most of the day. The aim of this work was to demonstrate that Hybridization of various renewable energy sources and battery bank is a key for system cost effectiveness and high performance than any other variant based on a single renewable source. The sizing results suggests that HOMER software is a powerful, efficient and flexible tool that gives the optimum and cost effective systems based on renewable source.

References

[1] Tiberiu T. &Alexandru, M., "Optimum Design of wind/PV/Diesel/Batteries Hybrid systems." 2008.

[2] M. Marvwan& H. ImadIbrik, "Techno- economic feasibility of energy supply of remotevillages as Palestine by PV- systems, diesel generators and electric grid," renewable and sustainable energy. Reviews pp 128-138, 2006.

[3] Sambo, A.S., International centre of energy, "Energy and Development Report, Renewable Electricity Action Program," federal ministry of power and steel, Nigeria 2006.

[4] Akpama, E.J.,"Designing a photovoltaic sustained sector: a review of current practice,"domestic use of energy conference, pp 155-160. 2011.

[5] Chimeka I. U, &chineke T. C. "Evaluating The Global Solar Energy Potential AtUturu, Nigeria."International journal of physical sciences.Vol.4(3), pp 115-119, 2011.

[6] Dusabe, J.L. Munda, &Jimoh A.A. "Small Scale Solar Energy System In Rwanda: Status. And Sustainability."Domestic use of energy conference, pp 137-141, 2009.

[7] Rogers A. Messenger, " photovoltaic" floridaatlantic university, 2006.

[8] G.D. Rai, "non-conventional energy sources."Khanna publishers 2-B,Nath market, NaiSarak Delhi-m110006. India.2008.

[9] Retrieved from " http://en.wikipedia.org/wiki/portal:Renewableenergy."

[10] Donald E.O. & David E.C., "Utility Grid-Connected Distributed Power Systems." National solar energy conference.ASES solar, 1996.

[11] Augustine C. &Nnabuchi M. N. "Relationship between Global Radiation And. Sunshine Hours ForCalabar, Port Harcourt And Enugu, Nigeria." International Journal of physical sciences vol. 4(4), pp.182-188, 2009.

IOSR Journal of Electrical and Electronics Engineering (IOSR-JEEE)
ISSN: 2278-1676Volume 3, Issue 3 (Nov. - Dce. 2012), PP 28-36
www.iosrjournals.org

ASR For Embedded Real Time Applications

K.Kartheek[1], D.V.Srihari Babu[2]
1. K. Kartheek, M.Tech, SKTRMCE,
2. D.V.Srihari Babu, M.Tech (Ph.D.), Assoc. Proff, S.K.T.R.M.C.E.,

Abstract: *The system consists of a standard microprocessor and a hardware accelerator for Gaussian mixture model (GMM) emission probability calculation implemented on a field-programmable gate array. The GMM accelerator is optimized for timing performance by exploiting data parallelism. In order to avoid large memory requirement, the accelerator adopts a double buffering scheme for accessing the acoustic parameters with no assumption made on the access pattern of these parameters. Experiments on widely used benchmark data show that the real-time factor of the proposed system is 0.62, which is about three times faster than the pure software-based baseline system, while the word accuracy rate is preserved at 93.33%. As a part of the recognizer, a new adaptive beam-pruning algorithm is also proposed and implemented, which further reduces the average real-time factor to 0.54 with the word accuracy rate of 93.16%. The proposed speech recognizer is suitable for integration in various types of voice (speech)-controlled applications.*

Index Terms: *Automatic speech recognition (ASR), embedded system, hardware–software codesign, real-time system, softcore-based system.*

I. Introduction

Automatic speech recognition (ASR) on embedded platforms has been gaining its popularity. ASR has been widely used in human–machine interaction, such as mobile robots, consumer electronics, manipulators in industrial assembly lines, automobile navigation systems, and security systems. More sophisticated ASR applications with larger vocabulary sizes and more complex knowledge sources are expected in the future. As a result, the demand for high performance, accurate, and fast embedded ASR is increasing. This approach enables fast deployment of ASR-based applications. However, the timing performance is constrained by the processing power and memory bandwidth of the target platforms. At another extreme, a speech recognizer can be tailor-made in a *pure hardware-based* system for good timing performance. However, in many human-machine interaction applications, the search space for decoding speech varies dynamically depending on the user's response. A dedicated hardware architecture with a static search space has limited capabilities to deal with the dynamic nature of ASR. In addition, the architecture becomes too application-specific and targets to only ASR applications. It is unlikely that the datapath of the hardware can be reused for applications other than ASR. As a compromise, a *hardware–software codesign* approach seems to be attractive. A typical hardware–software coprocessing system consists of a general purpose processor and hardware units that accelerate time critical operations to achieve required performance. Computationally intensive parts of the algorithm can be handled by the hardware accelerator(s), while sequential and control-oriented parts can be run by the processor core. The additional advantages of the hardware–software approach include the following:

1) Rapid prototyping of applications. Developers can build their applications in software without knowing every detail of the underlying hardware architecture.
2) Flexibility in design modification. The parts of the algorithm which require future modification can be implemented initially in software.
3) Universality in system architecture. The use of the general purpose processor core enables developers to integrate ASR easily with other applications.

In this paper, we present the development and tradeoffs of a hardware–software coprocessing ASR system which primarily targets on embedded applications. The system includes an optimized hardware accelerator that deals with the critical part of the ASR algorithm. The final system achieves real-time performance with a combination of software- and hardware implemented functionality and can be easily integrated into applications with voice (speech) control.

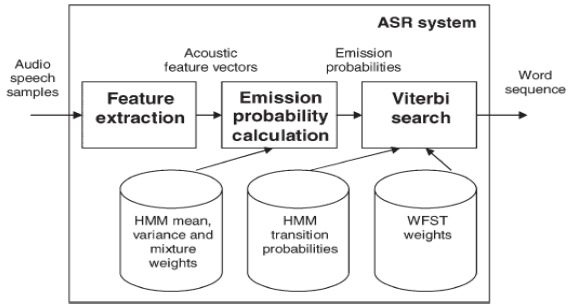

Fig.1. Data flow diagram of a typical ASR system. The input of the system is an audio speech signal. The output is a sequence of words.

II. Automatic Speech Recognition System

In a typical hidden Markov model (HMM)-based ASR system, three main stages are involved. Fig. 1 shows the data flow within the ASR algorithm. The first stage is *feature extraction*. Its main purpose is to convert a speech signal into a sequence of acoustic feature vectors, $\mathbf{o}^{\mathrm{T}}_1 = \{\mathbf{o}_1, \mathbf{o}_2, \ldots, \mathbf{o}_T\}$, where T is the number of feature vectors in the sequence. The entire speech signal is segmented into a sequence of shorter speech signals known as frames. The time duration of each frame is typically 25ms with 15ms of overlapping between two consecutive frames. Each frame is characterized by an acoustic feature vector consisting of D coefficients. One of the widely used acoustic features is called mel frequency cepstral coefficient (MFCC). Feature extraction continues until the end of the speech signal is reached. The next stage is the calculation of the *emission probability* which is the likelihood of observing an acoustic feature vector. The emission probability densities are often modeled by Gaussian mixture models (GMMs). The last stage is *Viterbi search* which involves searching for the most probable word transcription based on the emission probabilities and the search space. The use of weighted finite state transducers (WFSTs) offers a tractable way for representing the search space. The advantage is that the search space represented by a WFST is compact and optimal. Fig. 2 shows an example of a search space. Basically, a WFST is a finite state machine with a number of states and transitions. As shown in Fig. 2, each WFST transition has an input symbol, an output symbol, and a weight. The input symbols are the triphone or biphone labels. The output symbols are the word labels. In ASR, a word is considered as a sequence of subword units called phones. Two or three phones are concatenated to form biphones or triphones. Each triphone or biphone label is modeled by an HMM. In other words, each WFST transition in Fig. 2 is substituted by an HMM. The entire WFST is essentially a network of HMM states. The WFST weights are the language model probabilities which model the probabilistic relationship among the words in a word sequence. Usually, a word is grouped with its preceding $(n-1)$ words. The n-word sequence called n-gram is considered as a probabilistic event. The WFST weights estimate the probabilities of such events. Typical n-grams used in ASR are unigram (one word), bigram (two word, also known as word pair grammar), and trigram (three word). For implementation purposes, each HMM state has a bookkeeping entity called *token* which records the probability (*score*) of the best HMM state sequence ended at that state.Each token is propagated to its succeeding HMM states according to the topology of the search space. For example, in Fig. 2, the token in State 3 of the /k-ae+t/ HMM will replicate itself. One will propagate to its own state with HMM transition probability ($a33$ in this example) added to the token's score. Another replicated token will enter State 1 of the /ae-t/ HMM and the WFST weight ($\omega 6$) will be added to its score. When two tokens meet at an HMM state, only the better token with a higher score survives and stays at the HMM state. Other losing tokens are discarded. This method of performing the Viterbi search is known as *token passing*. In addition to a score, tokens also record a sequence of word labels encountered during propagation. The pseudocode of the ASR algorithm is shown in Fig. 3. In the beginning of the algorithm, a token is instantiated in each of HMM states at the start of each word (Line 2). Qword−start is a set of word-starting HMM states. The score of each token is reset (Line 3). After the initialization, the algorithm begins to process each frame of speech. An acoustic feature vector, $\mathbf{o}_t$, is generated by *feature extraction* (Line 6) for each speech frame. In practice, it is intractable to perform a complete Viterbi search over all the HMM states within the search space. Therefore, *pruning* is essential for practical applications with the cost of introducing search errors. One of the common pruning techniques is called *beam pruning*. A *pruning threshold* is determined by subtracting a certain value called *pruning beamwidth* from the maximum token score (Lines 8–9). A token remains active if its score is above the pruning threshold (Line 13). Otherwise, the token is discarded. Pruning is said to be tight when the pruning beamwidth is narrow, which reduces the number of active tokens in the search space. Since there are fewer tokens, the decoding time is shorter. However, the word accuracy rate tends to decrease in tight pruning since the token with the correct word transcription has a greater chance to be discarded.

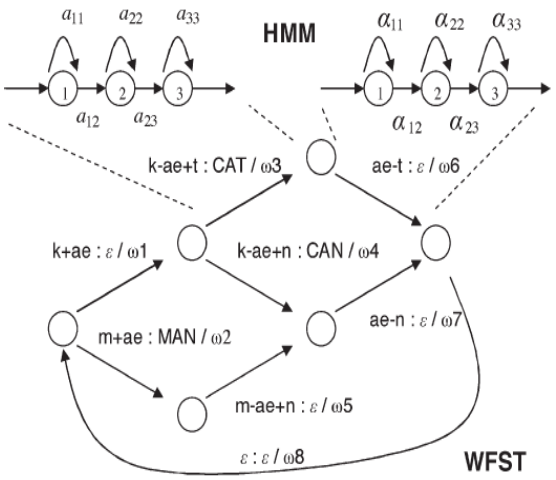

Fig. 2. Search space represented by a WFST. Each WFST transition *x* : *y/z* has three attributes. *x* is an input symbol representing a triphone or biphone label. *y* is an output label representing a word label.

Algorithm 1 Speech recognition algorithm

```
/* Q̃_t is a set of HMM states which have tokens at time t */
Q̃_1 ← Q_{word−start}
score_{q,1} ← 0 for all q ∈ Q̃_1

for t = 1 to T do
    o_t ← Feature_extraction(Frame_t)

    max_score ← max(score_{q,t}) for all q ∈ Q̃_t
    pruning_threshold ← max_score − pruning_beamwidth
    Q̃_{t+1} ← {}

    for all q ∈ Q̃_t do
        if score_{q,t} > pruning_threshold then
            log_emis_prob ← Emission_prob_calc(o_t, q)
            V ← Viterbi_search(log_emis_prob, q, t)
            Q̃_{t+1} ← Q̃_{t+1} ∪ V
        end if
    end for
end for

Q ← Q̃_{T+1} ∩ Q_{word−end}
best_token ← argmax_{q∈Q}(score_{q,T+1})
```

Fig. 3. Pseudocode of the speech recognition algorithm with beam pruning.

Algorithm 2 $\mathcal{V} \leftarrow Viterbi\_search(log\_emis\_prob, q, t)$

```
V ← {}
for all q_suc states that succeed State q do
    new_score ← score_{q,t} + log_emis_prob + trans_weight(q, q_suc)
    if new_score > score_{q_suc,t+1} then
        score_{q_suc,t+1} ← new_score
        path_{q_suc,t+1} ← path_{q,t}
        V ← V ∪ {q_suc}
    end if
end for
return V
```

Fig. 4. Pseudocode of the *V iterbi_search* function

After feature extraction and setting the pruning threshold, the algorithm iterates through all the HMM states that have a token (Lines 12–18). If the token stays above the pruning threshold, the *emission probability* of that state is calculated (Line 14). After that, *Viterbi search* is performed on that HMM state (Line 15). Token-passing takes place during this process. It returns a set of new HMM states, *V*, which are occupied by the new tokens after token passing. The new tokens are accumulated into another set ˜*Qt*+1 which is prepared for the next speech frame. Once all the speech frames have been processed, the best token is found among all the word-end HMM states denoted by *Q* (Lines 21–22). The best token records its propagation path from which the word transcription can be determined. Fig. 4 shows the pseudocode of the *V iterbi_search*() function. The for-loop iterates through all the succeeding states of *q* (Lines 2–9). For each succeeding state, *new_score* is calculated (Line 3) where the transition weight can be either the HMMtransition probability for within-HMM transitions or the WFST transition weight for cross-HMM transitions. If *new_score* is greater than the score at *q_suc*, the *new_score* will update the score at *q_suc* (Line 5). The path record of the original token at *q_suc* is replaced by the path record at *q* (Line 6). The pseudocode shows that there are three major levels of iterations in the ASR algorithm: 1) iteration of *T* speech frames (Line 5 in Fig. 3); 2) iteration of ˜*Qt* HMM states in each frame (Line 12 in Fig. 3); and 3) iteration of *qsuc* states for each active HMM state (Line 2 in Fig. 4). Since the search result of each speech frame in the first iteration loop depends on previous frames, only the second and the third loops are suitable for possible parallelism. However, data contention is likely to occur because an HMM state is often a *qsuc* state of multiple HMM states. The impact of contention on timing performance needs to be carefully studied if parallelism is adopted. The performance of an ASR system is often evaluated by two metrics. The first metric is word accuracy rate which is defined as follows [23]:

$$\text{Word accuracy rate} = \frac{n - s - d - i}{n} \times 100\% \quad (1)$$

where *n* is the total number of words. *s* is the number of word substitutions (incorrectly recognized words). *d* and *i* are the numbers of word deletions and word insertions, respectively. The second metric is real-time factor which measures the timing performance of the ASR system. It is defined as follows:

$$\text{Real-time factor} = \frac{\text{Decoding time}}{\text{Speech duration}}. \quad (2)$$

III. Hardware–Software Coprocessing System

The ASR algorithm is partitioned into three main parts: feature extraction, GMM emission probability calculation, and Viterbi search. The speech recognizer is first implemented in software where the 16-b fixed-point implementation of the recognizer is compared with the floating-point implementation. The experimental results show that there is no degradation in recognition accuracy in the fixed-point implementation. Hence, the fixed-point system is chosen as our baseline system for time profiling. It shows that about 69% of the total elapsed time is spent on GMM computation. The proportions of time spent on feature extraction and Viterbi search are 7% and 24%, respectively. Since GMM computation is the most computationally intensive part, a hardware accelerator is designed in order to speed up this part of the ASR algorithm.

A. System Architecture

The architecture of the hardware–software coprocessing system is shown in Fig. 5. The system consists of an Altera Nios II processor core and a GMM hardware accelerator. The Nios II processor acts as the control unit of the entire system. Feature extraction and Viterbi search are implemented in software. When the system needs to perform a GMM calculation, the processor instructs the accelerator to carry out the computation. The accelerator returns the computation result to the Nios II core. The entire coprocessing system is synthesized on an Altera Stratix II EP2S60F672C5ES field-programmable gate array (FPGA).

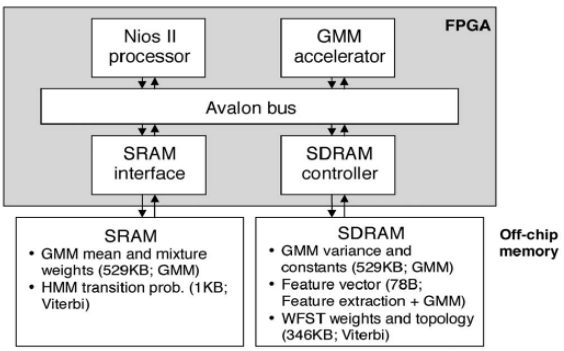

Fig. 5. System architecture of the hardware–software coprocessing recognizer with the GMM hardware accelerator. Inside the brackets, it shows the data size and the ASR substages in which the data are accessed. The Nios II processor performs feature extraction and Viterbi search, while the GMM accelerator is used for GMM computation.

B. GMM Emission Probability Hardware Accelerator

1) Datapath: The GMM hardware accelerator calculates the log emission probability of an observation vector given an HMM state. Given an observation feature vector $\mathbf{o}_t$, the emission probability function in an HMM state j is modeled by a sum of weighted Gaussian mixtures

$$b_j(\mathbf{o}_t) = \sum_{m=1}^{M} b_{jm}(\mathbf{o}_t) \qquad (3)$$

$$= \sum_{m=1}^{M} c_{jm}\mathcal{N}(\mathbf{o}_t, \boldsymbol{\mu}_{jm}, \boldsymbol{\Sigma}_{jm})$$

where $b_{jm}(\mathbf{o}t)$ is the probability density function of the weighted mth Gaussian mixture. $N(.)$ denotes a Gaussian mixture. The mean vector and the covariance matrix of the Gaussian mixture are denoted by $\boldsymbol{\mu}_{jm}$ and $\boldsymbol{\Sigma}_{jm}$, respectively. Since the coefficients of a feature vector are assumed to be independent, $\boldsymbol{\Sigma}_{jm}$ is a diagonal matrix. The total number of Gaussian mixtures is$M$ per HMM state. The weight of the mth Gaussian mixture is c_{jm}. The logarithm of a weighted Gaussian mixture, $\log b_{jm}(\mathbf{o}_t)$, can be expressed by the following equation:

$$\log b_{jm}(\mathbf{o}_t) = C_{jm} + g_{jm} + \sum_{d=0}^{D-1} \left(o_t^{(d)} - \mu_{jm}^{(d)}\right)^2 v_{jm}^{(d)}. \qquad (4)$$

In the equation, $o(d)$ t is the dth dimension of the observation vector at time t. D is the dimension of the observation vector. In many ASR applications, the typical value of D is 39, which is commonly adopted by the research community. $\mu(d)$ jm is the dth dimension of the $\boldsymbol{\mu}_{jm}$ mean vector. C_{jm}, $v(d)$ jm, and g_{jm} are constants defined as follows:

$$C_{jm} = \log c_{jm} \qquad (5)$$

$$v_{jm}^{(d)} = \frac{-1}{2\left(\sigma_{jm}^{(d)}\right)^2} \qquad (6)$$

$$g_{jm} = -\frac{1}{2}\left(D\log(2\pi) + \sum_{d=0}^{D-1} \log\left(\sigma_{jm}^{(d)}\right)^2\right) \qquad (7)$$

where the symbol ($\sigma(d)$ *jm*)2 is the *d*th feature variance, which is the *d*th diagonal element of the covariance matrix. The log emission probability, log *bj*(**o***t*), can be evaluated recursively by the following equation:

$$\log b_j(o_t) = ((\log b_{j1}(o_t) \oplus \log b_{j2}(o_t)) \oplus \ldots) \oplus \log b_{jM}(o_t). \quad (8)$$

The $\oplus$ symbol represents the *log-add* operator, which has the following definition and approximation:

$$x \oplus y = \log(\exp(x) + \exp(y)) \approx \begin{cases} y & z < -16 \\ y + \log(1 + \exp(z)) & -16 \le z < 0 \\ x + \log(1 + \exp(-z)) & 0 \le z < 16 \\ x & z \ge 16 \end{cases} \quad (9)$$

where $z = x - y$. When $|z|$ is greater than a threshold, the difference between exp(x) and exp(y) is large enough to just consider only the greater number. The threshold value of 16 is chosen because it shows no degradation in recognition accuracy and also it is a power of two. Several different thresholds (8, 16, and 32) are tested. The word accuracy rates stay at 93.33% for threshold values of 16 and 32, whereas there is a slight decrease in word accuracy (about 0.03%) when the threshold is 8. The log(1 + exp(.)) function can be calculated offline and stored in a lookup table. The $|z|$ value can be used as the look-up index of the table. It can be seen from (4) that there is a summation of *D* interim values. Since these values are independent of each other, it is possible to compute *N* of them at the same time in parallel, where $1 \le N \le D$. For example, if $N = D$, *D* interim values are calculated in one go. However, if $1 < N < D$, *N* interim values are calculated each time and it requires _*D*/*N*_ iterations to calculate all the values. In contrast, there is no parallelism if $N = 1$. In other words, the degree of parallelism is governed by *N*, and it is a design variable which needs to be optimally chosen. In order to avoid pipeline stalls, the hardware accelerator adopts a double-buffering scheme as shown in Fig. 6. Each buffer contains the GMM parameters of an HMM state. Since the Avalon bus is 32-b wide and there are two separate memories (SRAM and SDRAM), 8 B of parameters can be loaded to the buffer in each clock cycle. GMM calculation and Viterbi search are performed during the retrieval of the next HMM state parameters from the off-chip memories. The accelerator only needs to store the parameters of two HMM states, which are about 1280 B in the internal memory of the FPGA chip. Observation vector only needs to be loaded once for each speech frame. The size of the observation vector buffer is 78 B.

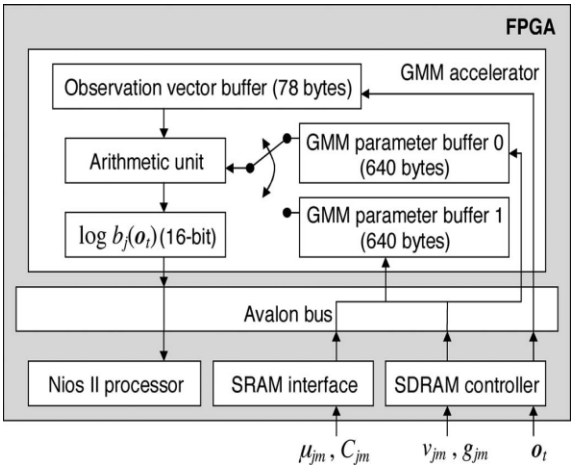

Fig. 6. Double-buffering inside the GMM hardware accelerator. The arithmetic unit is reading from one buffer while another buffer is retrieving GMM parameters from off-chip memories.

The major differences between the proposed system and the other coprocessing system are as follows:

a) The GMM accelerator has only one computation unit for calculating one dimension. We argue that this architecture is not optimized. The proposed system includes *N* computation units and a parallel adder block to further employ data parallelism.

b) The accelerator in their system computes log $b_{jm}(\mathbf{o}_t)$ only. The summation of Gaussian mixtures is done by the general purpose processor in software, while the proposed accelerator includes a hardware log-add unit and the final output is log $b_j(\mathbf{o}_t)$.
c) The accelerator in their system internally stores 128 kB of HMM parameters, which is about 20% of the total amount. This makes the architecture infeasible for larger vocabulary tasks. In addition, the parameters are predetermined. The parameters of the most probable HMM states, which are found by offline profiling on the test speech data, are stored inside the accelerator. In contrast, our proposed accelerator only stores two HMM states (1280 B). Furthermore, we do not make any assumptions on which HMM states should be stored.

2) Timing Profile:

After synthesis and place and route, the proposed system is implemented on the target FPGA board. The first experiment is to investigate the relationship between the speedup in GMM calculation and the number of parallel computation units (N). The aim is to find the smallest number of computation units with maximum speed up. Fig. 9 shows the number of clock cycles for GMM calculation versus the number of computation units. The task is the Resource Management (RM1) task, which consists of 1200 test utterances. The vocabulary size is 993. Triphone HMM models with three emitting states and four Gaussian mixtures per state are trained on 2880 utterances. Acoustic features are 39-D MFCCs with the zeroth coefficient plus their delta and delta–delta coefficients. The language model is word-pair grammar (bigram). In terms of word accuracy, the GMM accelerator is the exact implementation of the algorithm. Hence, the word accuracy rate is 93.33% which is the same as that of the pure software-based system.

3) Resource Usage:

Table II shows the resource usage of the GMM hardware accelerator. Adaptive Logic Module (ALM), which can be programmed to perform logic functions, is the building block of a Stratix II FPGA device. M4K RAM blocks on the FPGA provide on-chip memory storage. Hardware multipliers are also embedded on the FPGA.

IV. Adaptive Pruning

Our goal is to reduce the decoding time of those utterances which have a relatively greater real-time factor, while keeping the recognition accuracy of the other utterances. In order to fulfil this goal, an *adaptive* pruning scheme is proposed, where the pruning beamwidth is adaptive according to the number of active tokens.

A. Algorithm

Fig. 11 shows the pseudocode of the ASR algorithm with adaptive pruning. In the beginning, the beamwidth is initialized to a value (Line 4). Before token passing, the algorithm modifies the pruning beamwidth according to the number of active tokens, $n(\tilde{Q}t)$. If the number of tokens is greater than a threshold, τupper, a tighter beamwidth is adopted. The beamwidth is decreased by a certain amount denoted by δ (Lines 11–12). However, if the number of active tokens is smaller than another threshold, τlower, and also if the beamwidth is tightened previously, the beamwidth will be relaxed and its value will be increased by δ (Lines 13–16). The rest of the algorithm is the same as the one shown in Fig. 3. The proposed pruning scheme is more flexible than the narrow and fixed pruning scheme. The number of active tokens is often time varying in the duration of an utterance. The fixed pruning scheme applies a tight beamwidth throughout theentire utterance regardless of the number of active tokens. On the other hand, the adaptive scheme allows relaxation of the beamwidth in parts of the utterance where the workload is less heavy. In terms of implementation, the proposed adaptive scheme is simpler than histogram pruning. Implementing histogram pruning requires a sorted list of the token scores. For each token, the recognizer needs to perform an insertion sort which involves searching for the token's ranking in a sorted list of the previously iterated token scores. Maintaining the tokens in a sorted order is computationally intensive. In contrast, the adaptive pruning scheme only requires to record the number of active tokens and a few decision-making statements (if-statements) for adjusting the beamwidth once for every speech frame.

B. Timing Profile

Fig. 12 shows the real-time factor of the coprocessing system. Fixed beam pruning and adaptive beam pruning are compared. The beamwidth is held constant at 170 for the fixed beam-pruning scheme. In adaptive beam pruning, the *original_beamwidth* variable is also set to 170. The thresholds, τlower and τupper, are 1900 and 2300, respectively. The beamwidth adjustment value is 10 (δ = 10). These parameters are determined empirically. In the fixed beam-pruning scheme, about 94% of the utterances have a real-time factor below one.

When the adaptive beam-pruning scheme is used, this percentage increases to 99.75%. Only 3 out of 1200 utterances have a real-time factor above one. Compared with the fixed beam-pruning scheme, there is a small degradation in recognition accuracy which decreases from 93.33% to 93.16%.We have also tried to tighten the adaptive pruning scheme by adjusting τupper and τlower to smaller values (τupper = 1700, τlower = 1250), so that the real-time factors of all the utterances are below 1. The word accuracy rate reduces to 92.62%.

Algorithm 3 Speech recognition algorithm with adaptive beam pruning

```
/* Q̃_t is a set of HMM states which have tokens at time t */
Q̃_1 ← Q_{word−start}
score_{q,1} ← 0 for all q ∈ Q̃_1
pruning_beamwidth ← original_beamwidth

for t = 1 to T do
    o_t ← Feature_extraction(Frame_t)

    max_score ← max(score_{q,t}) for all q ∈ Q̃_t

    if n(Q̃_t) > τ_upper then
        pruning_beamwidth ← pruning_beamwidth − δ
    else if n(Q̃_t) < τ_lower then
        if pruning_beamwidth < original_beamwidth then
            pruning_beamwidth ← pruning_beamwidth + δ
        end if
    end if

    pruning_threshold ← max_score − pruning_beamwidth
    Q̃_{t+1} ← {}

    for all q ∈ Q̃_t do
        if score_{q,t} > pruning_threshold then
            log_emis_prob ← Emission_prob_calc(o_t, q)
            V ← Viterbi_search(log_emis_prob, q, t)
            Q̃_{t+1} ← Q̃_{t+1} ∪ V
        end if
    end for
end for

Q ← Q̃_{T+1} ∩ Q_{word−end}
best_token ← argmax_{q∈Q}(score_{q,T+1})
```

Fig.7. Speech recognition algorithm with adaptive beam pruning.

V. Conclusion

The proposed ASR system shows much better real-time factors than the other approaches without decreasing the word accuracy rate. Other advantages of the proposed approach include rapid prototyping, flexibility in design modifications, and ease of integrating ASR with other applications. These advantages, both quantitative and qualitative, suggest that the proposed coprocessing architecture is an attractive approach for embedded ASR. The proposed GMM accelerator shows three major improvements in comparison with another coprocessing system. First, the proposed accelerator is about four times faster by further exploiting parallelism. Second, the proposed accelerator uses a double-buffering scheme with a smaller memory footprint, thus being more suitable for larger vocabulary tasks. Third, no assumption is made on the access pattern of the acoustic parameters, whereas the accelerator has a predetermined set of parameters. Finally, we have presented a novel adaptive pruning algorithm which further improves the real-time factor. Compared with other conventional pruning techniques, the proposed algorithm is more flexible to deal with the time-varying number of active tokens in an utterance. The performance of the proposed system is sufficient for a wide range of speech-controlled applications. For more complex applications which involve multiple tasks working with ASR, further improvement of timing performance, for example, by accelerating the Viterbi search algorithm, might be required.

References

[1] A. Green and K. Eklundh, "Designing for learnability in human–robot communication," *IEEE Trans. Ind. Electron.*, vol. 50, no. 4, pp. 644–650, Aug. 2003.
[2] M. Imai, T. Ono, and H. Ishiguro, "Physical relation and expression: Joint attention for human-robot interaction," *IEEE Trans. Ind. Electron.*, vol. 50, no. 4, pp. 636–643, Aug. 2003.
[3] B. Jensen, N. Tomatis, L. Mayor, A. Drygajlo, and R. Siegwart, "Robots meet humans—Interaction in public spaces," *IEEE Trans. Ind. Electron.*, vol. 52, no. 6, pp. 1530–1546, Dec. 2005.
[4] H. Lam and F. Leung, "Design and training for combinational neurallogic systems," *IEEE Trans. Ind. Electron.*, vol. 54, no. 1, pp. 612–619, Feb. 2007.
[5] A. Chatterjee, K. Pulasinghe, K. Watanabe, and K. Izumi, "A particleswarm- optimized fuzzy-neural network for voice-controlled robot systems," *IEEE Trans. Ind. Electron.*, vol. 52, no. 6, pp. 1478–1489, Dec. 2005.

About the Authors

K. Kartheek,
M.Tech,
Sri Kottam Tulasi Reddy College
Of Engineering & Technology,
A.P, India

D.V.Srihari Babu,
M.Tech (Ph.D.),
Assoc. Proff,
Sri Kottam Tulasi Reddy College
Of Engineering & Technology,
A.P, India.

IOSR Journal of Electrical and Electronics Engineering (IOSR-JEEE)
ISSN: 2278-1676Volume 3, Issue 3 (Nov. - Dce. 2012), PP 37-41
www.iosrjournals.org

Multi-module Singular Value Decomposition for Face Recognition

Bhanu Prasad[1], Sharad Kulkarini[2]
1. BhanuPrasad, M.Tech, SKTRMCE,
[2.]SharadKulkarini, M.Tech, Head of the Department(ECE), SKTRMCE,

Abstract: *The paper introduces a face recognition method using probabilistic subspaces analysis on multi-module singular value features of face images. Singular value vector of a face image is valid feature for identification. But the recognition rate is low when only one module singular value vector is used for face recognition. To improve the recognition rate, many sub-images are obtained when the face image is divided in different ways, with all singular values of each image used as a new sample vector of the face image. These multi-module singular value vectors include all features of a face image from local to the whole, so more discriminant information for face recognition is obtained. Subsequently, probabilistic subspaces analysis is used under these multi-module singular value vectors. The experimental results demonstrate that the method is obviously superior to corresponding algorithms and the recognition rate is respectively 97.5% and 99.5% in ORL and CAS-PEAL-R1 human face image databases.*

Keywords: *face recognition; probabilistic subspaces analysis; multi-module; singular value decomposition;*

I. Introduction

In recent years, computer vision research has witnessed a growing interest in subspace analysis techniques. And the important problem is how to extract the valid discriminant features for face recognition. The Karhunen-Loève Transform (KLT) and Principal Component Analysis are examples of eigenvector-based reduction and features extraction. A maximum a posteriori (MAP) matching rule using a Bayesian similarity measure derived from dual probabilistic has been applied for face recognition in. These methods have the disadvantages of the recognition performance easily affected by the facial expressions, large pose and variable illumination. A number of improved methods have been proposed. For example, the method using combination of wavelet packets and PCA/LDA have improved the face recognition rate, and Gabor representation based on probabilistic subspaces analysis for face recognition have also gotten the improvement of the face recognition, and so on. Their success shows that the traditional approaches applied in the different feature spaces can get the better recognition performance. Singular value features of matrix are widely used in the data compression, signal processing and pattern analysis, because they have the following features: the good stability, the proportional and rotational invariant. The singular value features of face images are firstly applied to face recognition in. The research of showed enough information needed could not be gotten for face recognition by using only one module singular value decomposition of whole face and the more features must be extracted. The paper introduces the face recognition method based on multi-module singular value features and probabilistic subspaces analysis (MSVD+PSA). Firstly, the sub-images are obtain when the face image is divided in different ways, then all singular value of each sub-image is organized and used as the sample vector of the face image. Finally, the method of probabilistic subspaces analysis is applied to the all sample vectors of face images.The remainder of the paper is organized as follows: In Section 2, the idea of the proposed method is described. The experimental results are presented for the ORL and CASPEAL- R1 face image databases to demonstrate the effectiveness and robustness of our method in section 3.Finally, conclusions are presented in Section 4.

II. Our Face Recognition Method

A. Multi-module Singular Value Decomposition:

The singular value decomposition (SVD) is one of the most important tools of numerical signal processing. It is employed in a variety of signal processing application, such as spectrum analysis, filter design, system identification etc. In singular value decomposition it has several advantages of computational efficiency and robustness under noise conditions. Singular value decomposition of matrix A ($m\times n$) can be written as follows:

$$A = U\Lambda VT \quad (1)$$

Where$U$ -The columns of U are the eigenvectors of AAT.U is an $m\times m$matrix containing an orthonormal basis of vectors for both the columns space and left null space of A. For orbit correction, the orbit vector will be

expanded in terms of the basis vectors in *U*. In linear algebra, *U* contains the left singular vectors of *A*. *Λ* - The 'singular values' or 'principle gains' of *A* lie on the diagonal of *Λ* and are the square root of eigenvectors of both *AAT* and *ATA*, that is, the eigenvector in *U* and the eigenvector of *V* share the same eigenvalues. *V* – The rows of *VT* (columns of *V*) are the eigenvectors of *AAT*. s an $n \times n$ matrix containing an orthonormal basis ofvectors for both the row space and right null space of *A*. The column vector of corrector magnets vector will be expanded in terms of the basis vectors in *V*. *V* contains the right singular vectors of *A*. We introduce the method of multi-module singular value decomposition. The *i*-by-*i* sub-matrices *p A* (where *p* is the total number of sub-matrices, and if $i \times i \times p \neq m \times n$, the face image matrix A is filled by zero to ensure the both sides of the equation are equal) are gained when the face image matrix *A* is divided in different ways. The sub-matrices *p A* of face image are shown in Figure 1 when the modules *p* is 16.

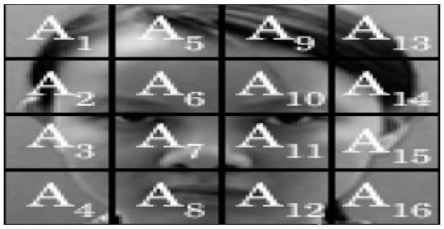

Figure 1. Example the face image is divided

The singular values (1,2, , , p) of all sub-matrices$A_k$are calculated by (1). Finally, the singular values $I_k$are organized as follows:

$$I = (I_1^T, I_2^T, \cdots, I_p^T)^T \qquad (2)$$

So, *I* (where the size of *I* is *i*-by-*p)* is used the sample vector of the matrix *A*. Because of the finite size of face image matrix A, the divided number of face image matrix A is also finite.

B. Probabilistic Subspace Analysis on the Singular Value of the Face Image:

Based on the above results, we obtain a training set of vectors $\{I\ t\}$, where $I \in RN = ip$and *t* is the total number of training sample, by lexicographic ordering of the pixel elements of each matrix. The basis function for the KLT are obtained by solving the eigenvalue problem

$\Lambda = \Phi T \Sigma \Phi$ (3)

Where Σ is the covariance matrix, Φ is the eigenvector matrix of Σ, and Λ is the corresponding diagonal matrix of eigenvalues. The unitary matrix Φ defines a coordinate transform (rotation) which de-correlates the data and makes explicit the invariant subspaces of the matrix operatorΣ. In PCA, a partial KLT is performed to identify the largest eigenvalue eigenvectors and obtain a principal component feature vector $y = \Phi_M^T \tilde{I}$,where $\tilde{I} = I - \bar{I}$ is the mean normalized vector and $\phi_M^T$is a sub-matrix of Φ containing the principal eigenvectors. PCA can be seen as a linear transformation $y = \Gamma(I) : R^N \rightarrow R^M$which extracts a lower dimensional subspace of the KL basis corresponding to the first M largest eigenvalues. These principal components preserve the major linear correlations in the data and discard the minor ones. By ranking the eigenvectors of the KL expansion with respect to their eigenvalues and selecting the first M principal components, we form an orthogonal decomposition of vector space R^Ninto two mutually exclusive and complementary subspaces: the principal subspace (or feature space) $\bar{F} = \{\phi_i\}_{i=M+1}^{N}$ containing the principal components and its orthogonal complement In practice there isalways a signal component in *F* due to the minor statisticalvariability in the data or simply due to the observation noisewhich affects every element of *I*.The complete likelihood estimate can be written as theproduct of two independent marginal

$$\hat{P}(\Delta \mid \Omega) = \left[\frac{\exp(-\frac{1}{2}\sum_{i=1}^{M} \frac{y_i^2}{\lambda_i})}{(2\pi)^{M/2} \prod_{i=1}^{M} \lambda_i^{1/2}} \right] \cdot \left[\frac{\exp(-\frac{\varepsilon^2(\Delta)}{2\rho})}{(2\pi\rho)^{(N-M)/2}} \right]$$
$$= P_F(\Delta \mid \Omega) \hat{P}_{\bar{F}}(\Delta \mid \Omega; \rho),$$

*(4)*Gaussian densitieswhere $P_F(\Delta|\Omega)$ is true marginal density in F, $P_F(\Delta|\Omega p)$ is theestimated marginal density in the orthogonal complement *F* ,$y_i$are the principal components, and $\varepsilon^2(\Delta)$ is the PCAresidual (reconstruction error). The information-theoreticoptimal value for the density parameter ρ is derived byminimizing the Kullback-Leibler (KL) divergence and isfound to be simply the average of the *F* eigenvalues

$$\rho = \frac{1}{N-M}\sum_{i=M+1}^{N}\lambda_i \quad (5)$$

In their formulation, the above expression for ρ is themaximum-likelihood solution of a latent variable model asopposed to the minimal-divergence solution.

C. Classification

We now consider the problem of characterizing the typeof differences which occur when matching two images in aface recognition task. We define two distinct and mutuallyexclusive classes: Ω_I representing intrapersonal variationsbetween multiple images of the same individual (e.g., withdifferent expressions and lighting conditions), and $\Omega_E$representing extrapersonal variations which result whenmatching two different individuals. We will assume that bothclasses are Gaussian-distributed and seek to obtain estimatesof the likelihood functions $P(\Delta|\Omega_I)$ and $P(\Delta|\Omega_E)$ for a givenintensity difference $\Delta = I1 - I2$ .Given these likelihoods we can define the similarity score$S(I_1,I_2)$ between a pair of images directly in terms ofintrapersonal a posteriori probability as given by Bayes rules:

(6)Where the priors $P(\Omega)$ can be set to reflect specific operatingconditions (e.g., numbers of test images vs. the size of thedatabase) or other sources of a priori knowledge regarding thetwo images being matched. Additionally, this particularBayesian formulation casts the standard face recognition task(essentially an M-ary classification problem for M individuals)into a binary pattern classification problem with Ω_I and Ω_E.This much simpler problem is then solved using the maximuma posteriori (MAP) rule——i.e., two images are determined tobelong to the same individual $P(\Delta|\Omega_I) > P(\Delta|\Omega_E)$, orequivalently, if $S(I_1,I_2) > 1/2$.

$$S = P(\Omega_I|\Delta) = \frac{P(\Delta|\Omega_I)P(\Omega_I)}{P(\Delta|\Omega_I)P(\Omega_I)+P(\Delta|\Omega_E)P(\Omega_E)}$$

III. Experimental Results

A. Experiment on the ORL Database

The proposed method is tested on ORL face database.Database has more than one image of an individual's face withdifferent conditions (expression, illumination, etc). There areten different of each of 40 distinct subjects. Each image hasthe size of 112×92 pixels with 256 levels of gray. For somesubjects, the images were taken at different times, varying thelighting, facial expressions (open/close eye, smiling/notsmiling) and facial details (glasses / no glasses). All theimages were taken against a dark homogeneous backgroundwith the subjects in an upright, frontal position (with tolerancefor some side movement). The original pictures of 112×92pixels have been resized to 64×64 so that the input space hasthe dimension of 4096.In our experiment, as five images are chosen for training,the remaining images (unseen during training) are used fortesting. Thus, the total number of training samples and testingsamples is 200, respectively. Training set is composed asfollows: the first five images in per class for training, namedSet 1; the behind five images in per class for training, namedSet 2. The final result is the average of the Set1 and Set2.As the modules of the face image increase, the recognitionrate is improved in Figure 2. When the modules are equal to121, the recognition performance achieves the best result. Butthe modules are more than 121, there is lower recognition rate.This shows the recognition performance are greatly affectedby the divided modules of original image, and the way ofcombination of multi-module singular value features andprobabilistic subspaces analysis can be improvement of therecognition performance.For comparison purpose, we first implemented theMSVD+PSA method, the MSVD+LDA method, and theMSVD + PCA method.We use the modules of the face imageare equal to 121 in the experiment, and the recognition rate isthe average of Set1 and Set2. The comparative facerecognition performance of these three methods is shown inFigure 3. One can see from the figure that the MSVD+PSAmethod performs better than other methods. Especially, whenthe number of features is very little,

the MSVD+PSA methodkeeps the high recognition rate.We compare the MSVD+PSA and PSA method (wherePSA method using the grey-value of original image). Theresult from Figure 4 show the MSVD+PSA method canachieve the recognition rate of 97.5%, but the PSA methodonly can get the best recognition rate of 94%. It also shows the MSVD+PSA method outperforms PSA.

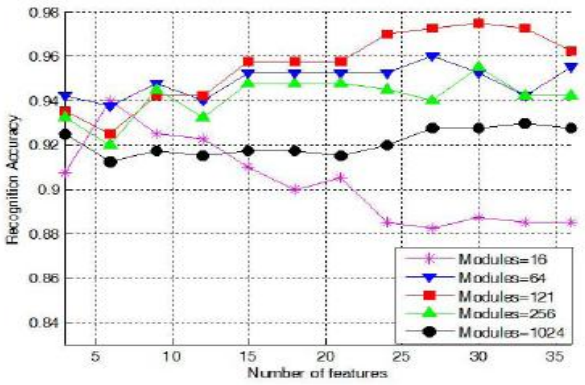

Figure 2. Recognition rate affected by different modules

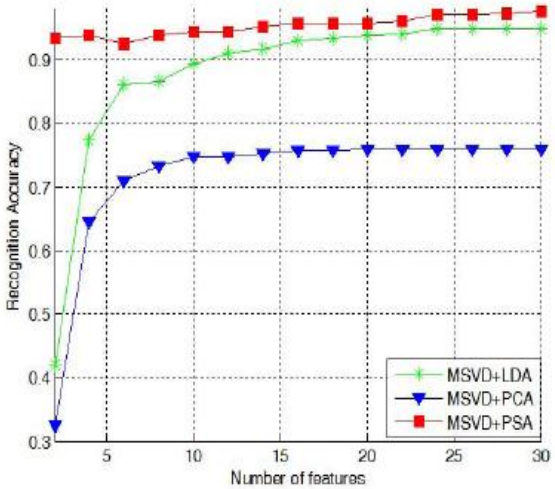

Figure 3.Comparative face recognition performance of the MSVD+PSAmethod, the MSVD+LDA method, and the MSVD + PCA method

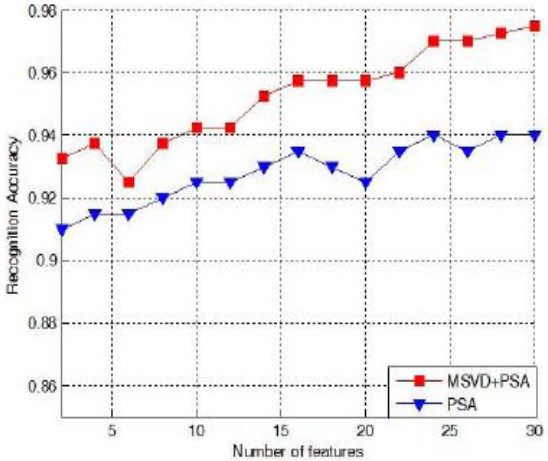

Figure 4. Comparative face recognition performance of the MSVD+PSA and PSA

B. Experiment on the CAS-PEAL-R1 Database

CAS-PEAL-R1 Database is a large face database,containing 30863 images of the 1040 subjects. Theexperiments involve 1200 face images corresponding to 200subjects such that each subject has six images of size 360×480 with 256 gray scale levels. The face image is cropped tothe size of 64×64 to extract the facial region, which is furthernormalized to zero mean and unit variance. Figure 5 showssome example images used in our experiments that are alreadycropped to the size of 64 × 64. Note that they especiallydisplay different facial expressions.

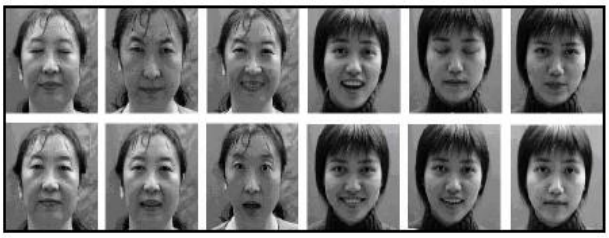

Figure 5.Example CAS-PEAL-R1 images used in our experiments.

IV. Conclusion

We have introduced in the paper a novel multi-modulesingular value features and probabilistic subspace analysisclassification. The proposed method, which is robust tovariations in illumination and facial expression, applies thePSA method to the organized singular value features derivedfrom the multi-module of the face image. These multi-modulesingular value vectors include all features of a face image fromlocal to the whole, so more discriminant information forpattern recognition is obtained. So the recognition rate of theproposed method for face recognition is higher than those ofother methods in the image domain. The feasibility of ourmethod has been successfully tested on face recognition usingORL and 1200 CAS-PEAL-R1 frontal face imagescorresponding to 200 subjects, which were acquired undervariable illumination and facial expressions. The novel ourmethod achieves respectively 97.5% and 99.5% accuracy onface recognition of ORL and CAS-PEAL-R1 face databases.

References:

[1] Tian Yuan, Tan Tie-niu, Wang Yun-hong. "Do singular values containadequate information for face recognition", Pattern Recognition, vol.36,no.6, pp:649-655, 2003.

[2] Esther Annlin Kala James, Dr.S.Annaduai, etal. "Implementation ofincremental linear discriminant analysis using singular valuedecomposition for face recognition", ICAC,2009.

[3] BabackMoghaddam, Alex Pentland. "Probabilistic visual learning forobject represention" , IEEE Trans. Pattern Analysis and MachineIntelligence, vol. 19, no. 7, pp. 696-710, July 2007.

[4] BabackMoghaddam. Watching Wahid and alexPenland. "Beyongeigenfaces: probabilistic matching for face recognition", proc. Int'l conf.Automatic Face and Gesture Recognition (FG'98),pp.30-35. Apr.1998.

[5] PN. Belhumeure, J.P. Hespanha, D.J. Kriengman, "Eigenfaces vs.fisherfaces: recognition using class spcific linear projection," IEEETrans. Pattern Analysis and Machine Intelligence, vol. 19, pp. 711-720,July 1997.

[6] W. .Gao, B.Cao, "The CAS-PEAL large-scale Chinese face database andbaseline evaluations," IEEE Transactions on Systems, Man, andCybernetics, vol. 38, pp. 149-161, January, 2008

About the Authors

Bhanu Prasad .P,
M.Tech,
Sri KottamTulasi Reddy College Of Engineering & Technology,

SharadKulkarni M.S(Ph.d)
Currently doing research on content based image retrieval in digital image processing stream.
Sri KottamTulasi Reddy College Of Engineering & Technology,

IOSR Journal of Electrical and Electronics Engineering (IOSR-JEEE)
ISSN: 2278-1676Volume 3, Issue 3 (Nov. - Dec. 2012), PP 42-45
www.iosrjournals.org

Sirpenski Carpet Fractal QR code

Anupam Tiwari
Member (L-20108), Institute of Electronics and Telecommunication Engineers- N Delhi

Abstract: *QR (Quick Reaction) code is 2 –dimension (2-D) mobile barcodes that are easily scanned using any modern mobile camera-equipped handsets/ phone to provide easy connectivity with internet. This QR Code will then be converted (called "dequrified") into a piece of (interactive) text and/or link. Presently QR codes are popular, because they are used for commercial tracking, logistics, inventory control, and advertising. In this paper two versions of Sierpinski Carpet are proposed as QR code. Sierpinski Carpet Fractal is well known Fractal and easy to generate. QR code, in Sierpenski pattern has main advantage of reduction of errors, easy generation, more symmetry, and enhanced data capacity. Sierpinski Carpet QR, the position for ensign is also better with definite scale (1/3rd) space generated by first iteration for putting ensign.*
Keywords: *Sierpenski Carpet, QR, Error code.*

I. Introduction

In present world people on move want to connect with internet with mobile devices. QR code is connect between mobile device containing camera with internet [1] .The basic QR code is a kind barcode with 2-D, of matrix symbol, which was developed by the Japanese company Denson-Wave in 1994. QR codes are used for Initiating a Web download, sending an SMS or email message, dialling a number, □ consuming data such as business card information directly from the code. Figure-1 shows the basic structure of QR code. There are quiet zone, position detection patterns, separators for position detection patterns, timing patterns, alignment patterns, format information, version information, data, and error correction code words. The main features of QR code contain large capacity, small printout size, high speed scanning, advanced error correcting, and freedom direction scanning. The overall are summarized as follows.

- High data capacity: QR code can store 7,089 numeric characters and 4,296 alphanumeric characters, and 1,817 kanji characters.
- High speed scanning: Smart phone/mobile with camera can get the content from a QR quickly and easily.
- Small printout size: QR Codes carry data on both horizontally and vertically, so due to 2-D is better as 1-D barcode.
- Advance error correcting: There is a 30% tolerance for error within any QR Code. The codes still can be recognized correctly as it is 2- D.
- Freedom direction scanning: QR can be scanned from any direction.

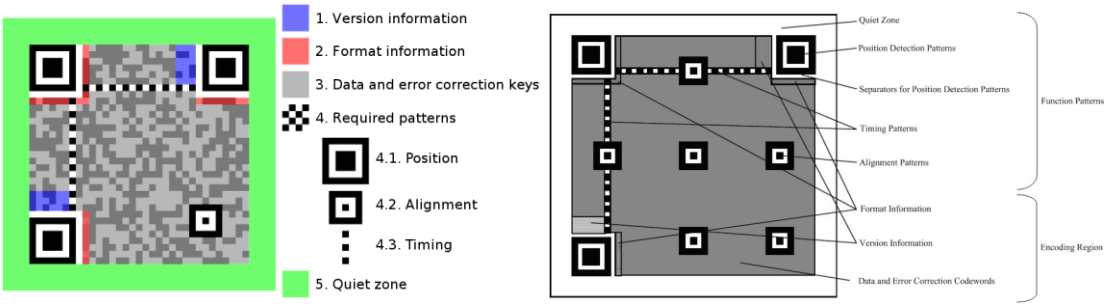

Figure-1

The QR code standard is fully described in the ISO/IEC 18004E International Standard and is available for purchase from the ISO Standard Organization for a nominal fee.

II. Existing Patterns Of QR Code

There are different patterns of Eye (square, diamond, etc), modules (Square, sieve, light roundness, etc) external eye colour, internal eye colour and background colour, foreground colours. Figure-2(Left) shows Diamond eye with foreground single colour blue. Shades of colour can also be used across length /breath or diagonal. Ensign can be also put at centre as shown in Figure -2 (Middle).

Figure-2(Left)

Figure-2(Middle)

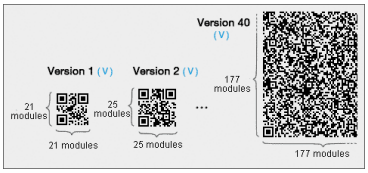

Figure-2(Right)

The standard specifies 40 versions (sizes) of the QR code from the smallest 21x21 up to 177x177 modules in size as shown in Figure-3(Right). The error level in QR code is as shown in the below table. The standard specifies four different principal schema, Numeric, Alphanumeric, Binary and Kanji as tabulated below.

Error level	Symbolic constant	Error correction capacity
L	Capacity::Er L	5 %
M	Capacity::Er M	15 %
Q	Capacity::Er Q	25 %
H	Capacity::Er H	30 %

Encoding mode	Maximum capacity
Numeric	7089 digits (Data matrix=3116)
Alphanumeric	4296 characters (Data matrix=2335)
Binary	2953 (Data matrix=1555)
Kanji	1817 (Data matrix NA)

Version	Modules	ECC Level	Data bits	Numeric	Alphanumeric	Binary	Kanji
1	21x21	L	152	41	25	17	10
		M	128	34	20	14	8
		Q	104	27	16	11	7
		H	72	17	10	7	4
Version	**Modules**	**ECC Level**	**Data bits**	**Numeric**	**Alphanumeric**	**Binary**	**Kanji**
40	177x177	L	23,648	7,089	4,296	2,953	1,817
		M	18,672	5,596	3,391	2,331	1,435
		Q	13,328	3,993	2,420	1,663	1,024
		H	10,208	3,057	1,852	1,273	784

$$W = (8*2 + (4V+1))\ X + 2Q$$

W= Width of QR code (including Quite zone), ***H***= Height of QR code (including Quite zone), ***X***= Width of QR Module, ***Q***= Width of the quite Zone; ***Q=4X***, ***V*** is the version which is 1 to 40.

Now, let us take**,** ***V*** max = 40, ***X*** min = 1, ***Q*** = 4***X***.

W max = (8 * 2 + (4***40**+ 1)) ***X*** + 2***Q***

= (177) ***X*** + 2 * 4***X***

= 177***X*** + 8***X***

= 185***X***

= 185pixel

III. Sierpenski Carpet Fractal

To construction of the Sierpinski Carpet Fractal begins with a square [2]. The square is cut into 9 congruent sub squares in a 3-by-3 grid, and the central sub square is removed this is first iteration. The same procedure is then applied recursively to the remaining 8 sub-squares, this process is infinite. The Hausdorff dimension of the carpet is log 8/log 3 ≈ 1.8928.

IV. Proposed QR Sierpenski Carpet

There are two Sierpenski Carpet QR code is proposed. First (left) is third iteration Sierpenski Carpet, the eye of QR code is kept at centre and alignment are nine green squares (remove centre square is first iteration, which can be used for ensign). Figure -3 is Sierpenski Carpet QR code, with quiet zone (Red boundary), version (blue horizontal bar), Timing (Red Squares), data and error code. The eye is at centre and green eight squares are for alignment. In Second (right) Sierpinski Carpet with three yellow positioned with one red alignment square. White squares for timing and sync, quite zone is outside the carpet. Data with error code can be put for rest of the location of carpet. Sierpinski Carpet is easily generated with small computer code program. Mathematically it is proved that this form of Fractal is compact and data storage can be enhanced with less error.

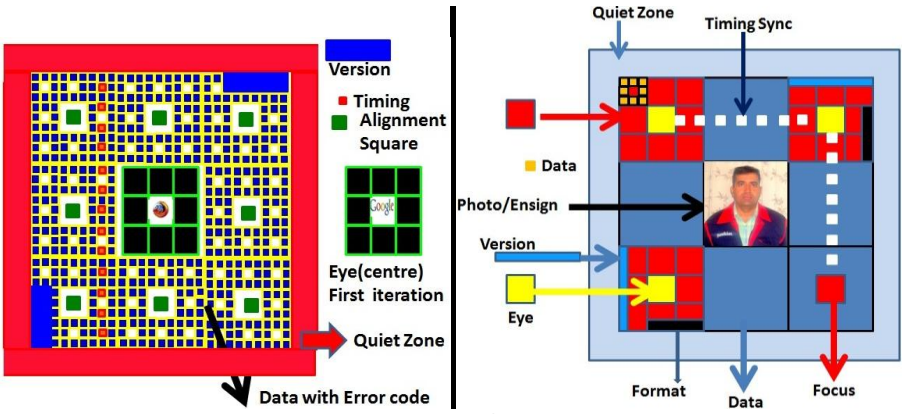

Figure -3

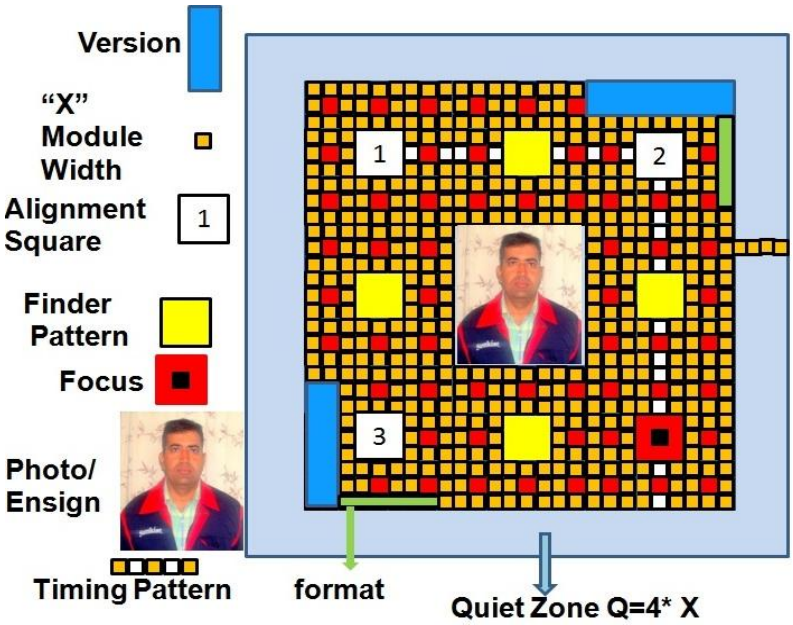

Figure -4 (Sierpinski Carpet QR Code with Ensign)

- With Sierpenski QR code, the main advantage of reduction of errors, easy generation, more symmetry and enhanced data capacity.
- Sierpinski QR is iterative so as per data iteration can be taken; Figure -4 is 3rd Iteration Sierpinski Carpet in which alignment pattern is three squares marked as 1,2and 3 and the ratio is 2:3:2. Extra finder pattern is of yellow squares.
- Sierpinski QR is more beautiful with good aesthetic look. Synchronisation and timing data frame doesn't interfere with alignment pattern. Centre unused square can be utilised for logo, thus logo doesn't reduce data space.
- Version and Module as per data can be selected, if more data then "Seed" dimension can be increased as shown in Figure-5. As per data dimension of seed can be fixed.
- Format and masking can be put as per data and requirement of contrast. Sierpinski Carpet QR code is having better masking as compared to ordinary black and white QR code.

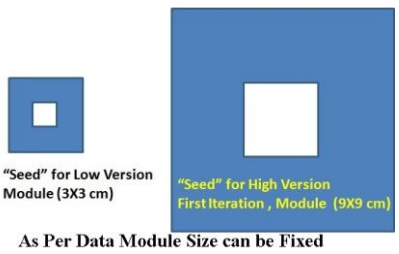

Figure -5 Versions and Module as per Data requirement

Version	Modules	ECC Level	Data bits
Low	(3cmX 3 cm)	L	As per iteration
High	(9 cm X 9 cm)	H	As per iteration

V. Conclusion

QR codes are presently growing their popularity because they connect mobile device with internet very easily. They are used for commercial tracking, logistics, inventory control, and advertising. Sierpinski Carpet Fractal QR code is proposed for QR codes as it is easy to generate by computer, Sierpinski Carpet is compact for data storage and unused center can be used for ensign. Depending on data size and iteration can vary, as iteration and size increases more data can be put with less error.

References

Journal Papers:

[1] K. Kiani, E. Kosari, and M. R. Simard, A New Method of Fractal Barcodes Identification, *Proceedings of the World Congress on Engineering and Computer Science 2011 Vol I WCECS 2011, October 19-21, 2011, San Francisco, USA*

Books:

[2] Heinz-otto Peitgen, D. S *Chaos and fractals new frontiers of science* (Springer-Verlag, 1992).

Bio data of The author

[3] Bio-data and e-mail is in QR code, (Please download free QR code from internet to decode bio-data), of Anupam Tiwari, or contact e-mail –anupamtiwari1972@rediffmail.com.

IOSR Journal of Electrical and Electronics Engineering (IOSR-JEEE)
ISSN: 2278-1676Volume 3, Issue 3 (Nov. - Dec. 2012), PP 46-55
www.iosrjournals.org

UV Spectrophotometer Based AI Techniques for Remnant Life Estimation of Power Transformers

Satyaprakash Ram[1], Dr. A.K. Chandel[2], Gurmeet Singh[3], Mithun Mondal[4]
[1,2,3,4] *(EED, National Institute of Technology, Hamirpur (H.P), India)*

***Abstract**: Power transformers are critical equipment in the electrical power system. Diagnostic and condition monitoring is very important for testing of power transformer oil in order to find the remnant life and has to be done carefully. Mineral oil in transformer serves two purposes the insulating as well as cooling and it is inseparable material of dielectric insulation system. The oil gets contaminated mainly due to ageing. The contaminant which changes the oils chemical and physical properties are moisture, acids, metal particles, sludge, and other compounds which are present in cellulose and due to aging insulation of the cellulose. UV-Spectrophotometer response is a nonintrusive test used to determine the transformer integrity and the response can be measured instantly with relatively cheap equipment and there is no need for an expert person. The present paper introduces two approaches of AI techniques they viz. Fuzzy logic and Artificial neural network (ANN) to estimate the relationship between dissolve decay content and UV spectrophotometer response of transformer oil method to determine the remnant life of the transformer oil. These two methods use the UV spectrophotometer bandwidth and absorbance values of the transformer oil as the inputs which are in service at several locations.*

***Keywords:** Artificial Neural network (ANN), Dissolve Decay Contents, Fuzzy logic, Transformer oil, UV Spectrophotometer.*

I. Introduction

Power transformer is extremely important electrical equipment in the power system as well as in industries. Transformers are vital links in transmission and distribution system. Proper maintenance of the transformer is able to decrease maintenance personnel requirements, improve reliability and security of power supply. The condition of the transformer oil reflects the health condition of the transformer because all the energized and high temperature components are immersed in the oil. In high voltage (HV) transmission and distribution systems, transformer oil is widely used as dielectric medium in HV power apparatus such as transformer, switchgear, current transformer, potential transformer etc. It has been estimated that every year about 30 to 40 billion litres of insulating oil is used as a dielectric medium in transformers in the world [1]. Since the transformers are one of the most important power equipments in electrical systems and also the costliest, hence they need to be monitored periodically to prevent any potential fault inside the transformer.

To minimize the capital expenditure of electrical power system, it is very common to operate these equipments at their limits of design parameters. Its failures create losses of revenues and catastrophic will create substantial costs in terms of the connected equipment destruction, environmental damages and unexpected used of resources. Regular monitoring is very important in order to find the remnant life of the transformer. Under the influence of thermal and electrical stresses, oil and oil-impregnated electrical insulating materials can be decomposed and generate some hydrocarbon gases which dissolve in mineral oil. The content of dissolved decay products in insulating oils is made up of a variety of compounds, such as peroxides, aldehydes, ketenes and organic acids [2]. Each of them is partially adsorbed on the large surface of paper insulation leading to the premature aging of power transformers. Hence, these by products can be used as an indicator of the aging of the mineral oil.

UV spectrophotometer is used to describe the relative level of dissolved decay products in transformer insulating oils which are of petroleum origin. If new oil is tested then it is almost transparent to the monochromatic beam of light in the visible spectrum, the increasing concentration of dissolved decay products shift the absorbance curve to longer wavelengths as shown in Fig. 3a to 3d [3-4]. This test method is applicable to compare the extent of dissolved decay products for oils in service. There is a relationship exists between the area under the absorbance curve and the total amount of dissolved decay products in mineral insulating oils. If the curve between the absorbance and wavelengths shift to longer then it indicates an increased content of dissolved decay products in the oil, while shift of the curve between absorbance and wavelengths is shorter then it indicates the selective removal of dissolved decay products. This paper introduces two methods to determine the dissolved decay product in mineral insulating oils of power transformers for remnant life estimation mathematically by Fuzzy logic and ANN (Artificial neural Network).

II. Spectrophotometer Method And Oil Sampling Techniques

An absorbance spectrophotometer measures the fraction of the incident light transmitted through a solution. It measures the amount of light that passes through a sample material and by comparison to the initial intensity of light reaching the sample, they indirectly measure the amount of light absorbed by that sample. Spectrophotometers are designed to transmit light of narrow wavelength ranges. As different compounds absorb light at different wavelengths, a spectrophotometer can be used to distinguish compounds by analyzing the pattern of wavelengths absorbed by a given sample. Additionally, the amount of light absorbed is directly proportional to the concentration of absorbing compounds in that sample, so a spectrophotometer can also be used to determine concentrations of compounds in solution. The amount of light transmitted through a solution is referred to as transmittance (T) [3].

The transmittance is defined as the ratio of the light energy transmitted through the sample (I) to the energy transmitted through the reference blank (I_0). Since the compound being tested is not present in the reference blank, the transmittance of the reference blank is defined as % T.

$$\%T = \frac{I}{I_0} \times 100 \tag{1}$$

Where,
T is transmittance,
I is light energy transmitted through the sample,
I_0 is the energy transmitted through the reference blank.

A certain portion of the light will be absorbed by the compound in the test cuvette; therefore its %T will be lower than that of the blank. The Lambert-Beer law, provides a linear relationship between absorbance and concentration of an absorber of electromagnetic radiation such as [3-4]

$$A = \varepsilon.l.c \tag{2}$$

Where,
ε = the extinction coefficient of the substance, has units of $\mathrm{M}^{-1} \times cm^{-1}$ (unique for each substance),
l = the sample path length measured in centimetres (the width of the cuvette almost always 1 cm),
c = the molar concentration of the solution (concentration in terms of molarities),

A_λ also referred to as Optical Density or OD_λ where λ is the wavelength used for the measurements.
Absorbance is related logarithmically to transmission

$$A = -\log(T) \tag{3}$$

$$A = -\log(I/I_0) \tag{4}$$

The absorbance of the reference blank is set at zero (A_λ= 0). The λ subscript is often dropped with the understanding that a value for ε is for a specific wavelength. If multiple species that absorb light at a given wavelength are present in a sample, the total absorbance at that wavelength is the sum due to all substances. Absorbance is additive

$$A_{Total} = A_1 + A_2 + ... \tag{5}$$

$$A_{Total} = \varepsilon_1 l c_1 + \varepsilon_2 l c_2 + ... \tag{6}$$

UV spectrophotometer has been used for last 35 years and over this period has become most important analytic instrument. The UV spectrophotometer provides reasonable information on the power transformers to plan relocation and operational criteria.

1.1 Oil samplings

Total 12 numbers of different transformer oil samples are collected from the Himachal Pradesh Electricity Board (HPSEB), India as per ASTM STD D-6802. The transformers ratings ranges from 5-50 MVA and their voltage ratios ratings are 132/33/11 KV. The oil samples are collected on the year's basis. The transformer oil sample which are collected are as one sample of 5 MVA transformer, two samples are of 7.5 MVA transformer and three samples each of 25 MVA, 45 MVA, 50 MVA transformers. The transformer oil samples collected are from new to old or aged oil samples of last past 8 to 10 years. The data is collected from the transformers maintenance records of the operation and maintenance department. The transformers have different service periods and aging conditions.

III. Experimental Setup and Procedure for UV Spectrophotometer

The experiment is done to find the dissolve decay content concentration of various samples of transformer oil. The experiment has been done according to ASTM D-6802. Initially, clean the cuvettes with the petroleum spirits or the same transformer oil sample. Adjust the UV Spectrophotometer to zero with spectral grade heptanes. This test is carried out at room temperature in the range 20°C to 30°C. During this process heptane is placed in 10mm path length glass cuvette, which is installed in UV spectrophotometer. The Heptane filled cuvette is then placed to the reference position in the instrument. The second glass cuvette is filled with the transformer oil sample which has to be tested [3]. The cuvette holder and cuvette containing the Heptane and transformer oil is shown in Fig.1.

Fig.1. Cuvette holders with heptane and oil

The cuvette with oil sample is placed so that the absorbance curve of the mineral oil can be determined. The absorbance curve is obtained from the instrument which scans in the range of 360-600 nm. The graph which is obtained is between wavelength and absorbance of the given oil samples. The relationship exists between the absorbance curve and the total amount of dissolve decay products in mineral insulating oil. The absorbance curve to the narrow wavelength indicates that the oil is new. If the curve between the absorbance and wavelengths shift to longer then it indicates an increased content of dissolved decay products in the oil, while shift of the curve between absorbance and wavelengths is shorter then it indicates the selective removal of dissolved decay products. Thus it indicates the condition of transformer oil. The complete setup of the procedure discussed above is shown in Fig. 2.

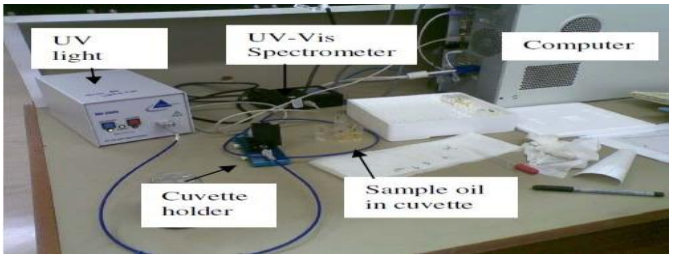

Fig.2 Setup for UV Spectrophotometer test

The assembly shows the complete setup of UV Spectrophotometer, the function of each equipment has been explained above. The graphs obtained from the UV Spectrophotometer for different oil sample are shown in Fig.3. Fig. 3(a) shows the UV spectrophotometer plot obtained from the Heptane sample which forms the base line. This is done to fulfil the zero condition of the instrument by adjusting it to read zero absorbance. The value obtained is constant and is equal to -0.092. The wavelength which the instrument is scan is in range of 360-600nm.

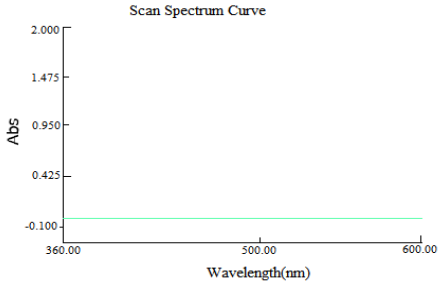

Fig.3 (a)

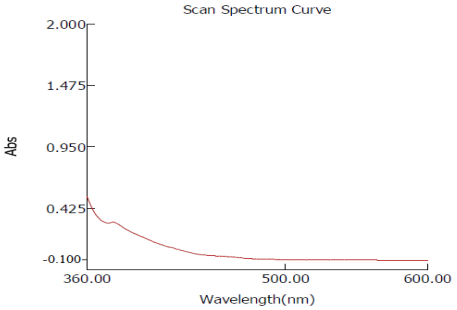

Fig.3 (b)

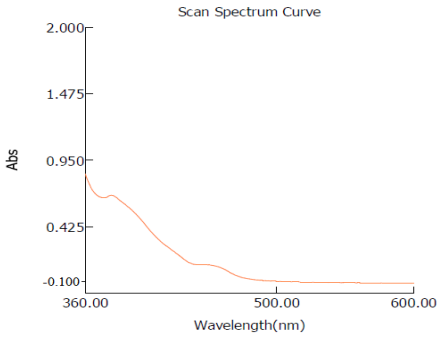

Fig.3 (c)

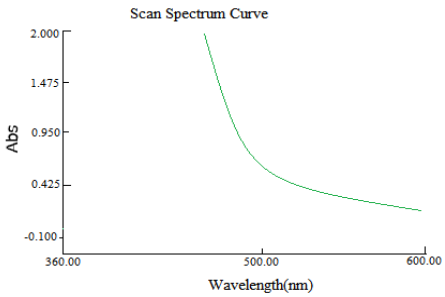

Fig. 3 (d)

Fig. 3. The graphs from the UV Spectrophotometer for different oil sample are (a) Show the base line (heptane) (b) Fresh transformer oil (c) Medium aged transformer oil (d) highly aged transformer oil.

Fig. 3(b) shows the UV Spectrophotometer plot obtained for fresh oil sample. For obtaining this graph the heptane-filled cuvette is moved to the reference position as mentioned previously. Now the second glass cuvette which is filled with the transformer oil sample is placed into the sample holder, and the UV scan is started. In Fig. 3(b) it is seen that there is a shift of the curve obtained from UV scan. It is seen that absorbance value is decreased from wavelength 360-600nm. Such behaviour of the change in the shift of the absorbance curve indicates that the oil is fresh. The UV Spectrophotometer plot obtained for medium aged transformer oil is shown in Fig. 3(c). The initial value of the absorbance has increased compared to the value in 3(b). The curve between the absorbance versus wavelength has been deviated more than the Fig.3(c), which indicates the presence of the dissolve decay products and impurities in the oil. As seen from the Fig.3 (d) that the curve between wavelength and absorbance had been increased to very high, this UV Spectrophotometer plot obtained is for highly aged transformer oil.

The absorbance curve which is obtained from this graph after UV scan indicates that there is increased content of dissolved decay products in transformer oil. An overall observation of all the plots obtained from the UV spectrophotometer shows that the curve shifts from the lower to higher side if there is a presence of impurities in the sample oil. The efficiency of the method will be high if it is possible to automatically identify the age of the oil. It will be more useful to the technicians if the information about the age of the oil is identified automatically. Hence, the decisive output regarding age of the oil in terms of characteristics like new oil, medium aged oil and highly aged oil is more useful [5].

For designing an automatic system the parameters obtained from the UV Spectrophotometer scan can be used. The age of the oil is classified as new, medium and highly aged oil. If the oil which is not in commission or of about 1 year age and if the dissolve decay content is very low then it is categorized as new oil. The oil which is tested about 5 to 7 years and if the dissolve decay content is normal to medium then it is categorized as medium aged oil. Finally, the oil sample tested after 9 to 10 years or more and if dissolve decay contents are very high then it is categorized as highly aged and it is required to be monitored. The aging depends on their contamination in the oil not on the basics of years.

IV. Transformers Life Estimation Techniques

In the present work two techniques viz. Fuzzy logic and ANN based techniques are proposed to determine the remnant life of the transformers by determining the dissolve decay contents present in the transformer oil. The details of the techniques used are as given below and there results are discussed in later section.

4.1 Fuzzy Logic Model

In this section, fuzzy logic model is developed to estimate the correlation of dissolve decay contents in transformer oil and its spectral response parameters. Results of the fuzzy logic model will be then compared to the results of ANN model. Input variables for the model are the values of bandwidth wavelength and the maximum absorption for different oil samples collected from the test set-up shown in Fig.1. The output from the model is the estimated dissolve decay content in ppm (parts per million). The model is built using the graphical user interface tool provided by MATLAB [6]. Each input was fuzzified into five sets (low to extensive) [7] of Gaussian combination membership function (MF) governed by the following equation

$$f(x,c,s,m) = \exp\left[\frac{1}{2}\left|\frac{x-c}{s}\right|^{m}\right] \qquad (7)$$

Where c is centre, s is width and m is Fuzzification factor. The function set developed for each input is a combination of s and c parameters. The corresponding Fuzzy logic simulation model developed is shown in Fig.4. The corresponding Gaussian function curves for each input variable are shown in Fig.5. And the corresponding Gaussian function curve for output variable is shown in Fig.6. Result of fuzzification from each input was then applied with fuzzy operator in the antecedent and related to the consequence, by IF- AND –THEN application method [8-9]. Centre of gravity which is widely used in fuzzy models was used for defuzzification method where the desired output z_0 is calculated as

$$Z_o = \frac{\int z.\mu_c(z)dz}{\int \mu_c(z)dz} \tag{8}$$

Where m_c (z) is the MF of the output.

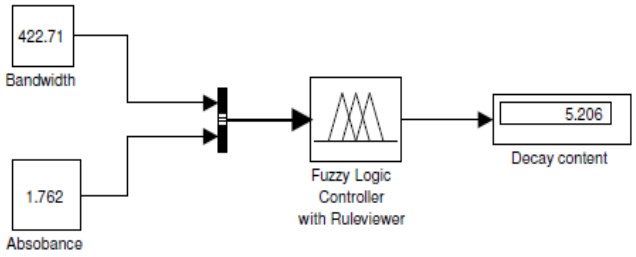

Fig.4 Fuzzy logic model for decay content estimation

The Fuzzy logic model developed using matlab simulation toolbox to estimate the remnant life of the power transformer by determining the dissolve decay contents in the transformer oil is shown in fig.4. It uses the Bandwidth and Absorbance values as the input and the dissolve decay content in ppm (parts per million) as the output. The model developed can be used for any input and output values which are in their ranges and it can be extended as desired.

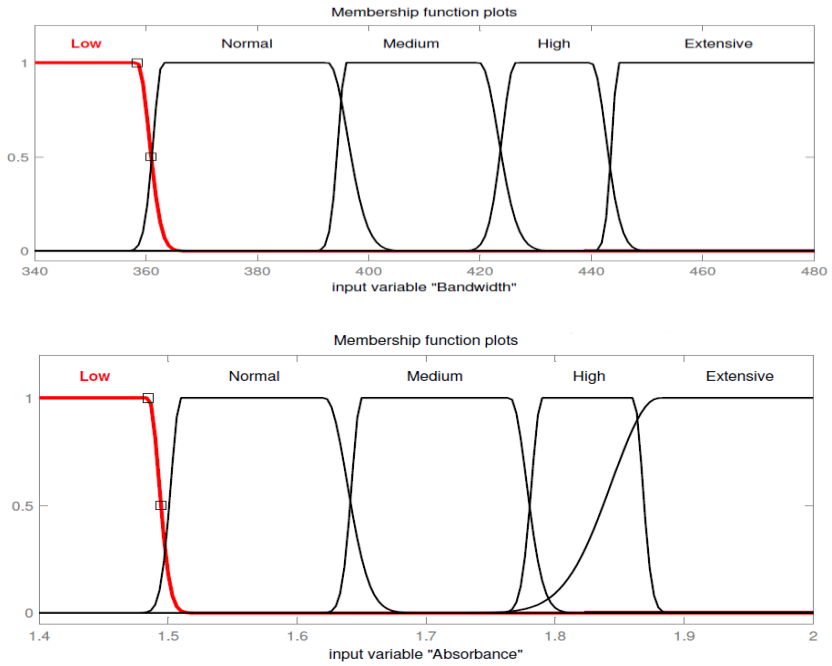

Fig.5 Input variable Membership Functions (bandwidth and absorbance)

The input membership functions for Bandwidth and Absorbance is shown in fig.5 and the membership functions (MF) used is the Gaussian MF function. The function is divided in five sets as low, normal, medium,

high and extensive. Bandwidth wavelength ranges from 340nm to 480nm and Absorbance ranges from 1.4nm to 2nm.

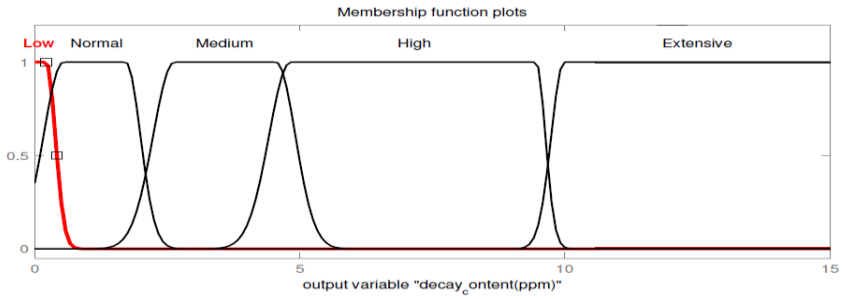

Fig.6 Output variable Membership Function (decay content)

The output variable membership functions is shown in Fig.6. The MF used is Gaussian MF and is fuzzified in five sets as that of the inputs. The output is dissolve decay content which ranges from 0ppm to 15ppm.

4.2 Artificial Neural Network

In this section the neural network simulation is developed using Matlab to estimate the correlation of dissolve decay content and the spectrophotometer response of the transformer oil [6]. Artificial Neural networks are a relatively new artificial intelligence technique. An artificial neural network (ANN) is determined by its architecture, training method and exciting function. Its architecture determines the pattern of connections among neurons. The neurons are connected by links and each link has a numerical weight associated with it. Weights are the basic means of long-term memory in ANNs. They express the strength or importance of each neuron input. Network training changes the values of weights and biases in each step in order to minimize the mean square of output error. Multi-Layer Perceptron (MLP) has been used in load forecasting, nonlinear control, system identification and pattern recognition [2-10], thus in this paper multi-layer perceptron network (with two inputs, one outputs and a hidden layer) with Levenberg-Marquardt training algorithm have been used.

4.2.1 Architecture and input-output of ANN

A multilayer perceptron is a feedforward neural network with one or more hidden layers. The input signals are propagated in a forward direction on a layer-by-layer basis. In the Fig.7 a multilayer neural network with two hidden layer has been shown [11]. The Matlab model developed was with the twenty two numbers of neurons in the hidden layer.

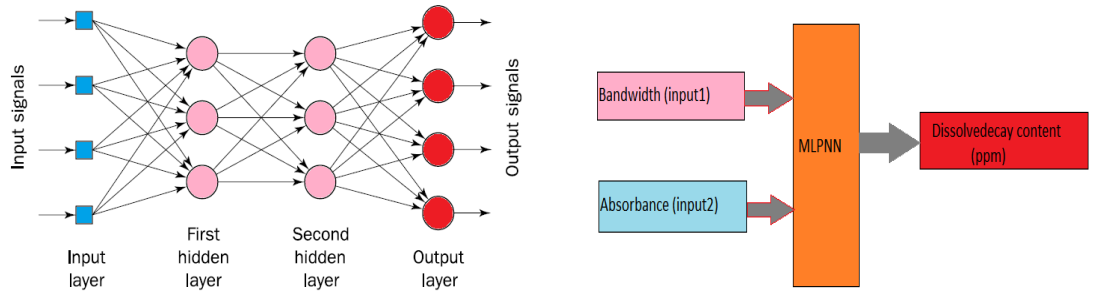

Fig.7 Multilayer perceptron with two hidden layers and Inputs and Output of ANN

For the neural network the input and output is required, so the spectrophotometer response with Bandwidth and Absorbance are given as input signals where as the dissolve decay content as the output signal. A typical network with input and output is shown in Fig.7.

ANN is made up of a hierarchy of layers, and the neurons in the networks are arranged along these layers. The neurons connected to the external environment form input and output layers. The weights are modified to bring the network input/output behaviour into line with that of the environment. Each neuron is an elementary information-processing unit. It has a means of computing its activation level given the inputs and numerical weights. To build an artificial neural network, we must decide first how many neurons are to be used and how the neurons are to be connected to form a network. Then we decide which learning algorithm to use and finally we train the neural network.

The back propagation training algorithm is a method of iteratively adjusting the neural network weights until the desired accuracy level is achieved. It is based on a gradient- search optimization method

applied to an error function. The network has been trained with Levenberg-Marquard back propagation algorithm. The number of neurons in hidden layer is twenty two.

V. Results and Discussions

Data for the methodologies as described in section 4 are generated according to the procedure given in section 3 of the paper. A total number of 12 transformer oil samples are taken for the study purpose. Using spectrophotometer the transformer oil samples are tested and obtained results are given in Table 1.

Table1. Results of UV Spectrophotometer

Oil samples	Bandwidth (nm)	Absorbance (nm)	Dissolve Decay Contents (ppm)
1	355.23	1.540	0.500
2	365.38	1.560	1.000
3	382.54	1.642	2.000
4	395.82	1.681	3.000
5	410.33	1.742	4.000
6	422.71	1.762	5.000
7	433.82	1.789	7.000
8	443.51	1.821	10.000
9	450.21	1.850	11.000
10	456.23	1.873	12.000
11	463.25	1.932	13.000
12	473.81	1.961	15.000

The dissolve decay content is in the range 0ppm to 15ppm. When the dissolve decay content for the transformer oil is reached to more than 12ppm that means its life has reduced and it needs to be maintained. The Fuzzy logic model which is developed using Matlab graphical user inference is with the accuracy of more than 95%. The ANN network model which is trained using Levenberg-Marquardt back propagation algorithm was able to correlate with dissolve decay content with accuracy more than 99%. The results obtained from the Fuzzy logic model and ANN model are compared with Spectrophotometer results which is shown in Table 2. The fuzzy logic model results are given in column 3 and ANN results are given in column 4 of Table 2.

Table2. Comparison of Fuzzy and ANN model with UV Spectrophotometer results

Oil samples	Target	Fuzzy Model output	ANN model estimated output	ANN Model Absolute Error
1	0.500	0.98	0.496	0.004
2	1.000	1.09	0.994	0.006
3	2.000	2.48	2.000	0.000
4	3.000	3.57	3.002	0.002
5	4.000	3.60	4.001	0.001
6	5.000	5.21	5.000	0.000
7	7.000	7.22	7.000	0.000
8	10.000	9.80	10.000	0.000
9	11.000	12.30	11.000	0.000
10	12.000	12.40	11.998	0.002
11	13.000	13.58	13.000	0.000
12	15.000	13.78	14.890	0.110

The ANN model Absolute Error is found by following formula

$$\text{Absolute Error} = |\text{ANN output} - \text{Target}| \quad (9)$$

The Fuzzy logic results are graphically shown in Fig.8 and Fig.9. The variation range in wavelength and absorbance and the corresponding decay content concentration are used to develop a set of fuzzy logic rules in the form of (IF-AND-THEN) statements to relate the input variables to the output, the rules are shown in Fig.8. The number of rules developed are 25 and the corresponding three dimensional graph obtained from Matlab is shown in Fig.9. The results which obtained using Fuzzy logic are with accuracy more than 95%. The examples of the rules developed are as follow.

1. If Bandwidth is low and Absorbance is low then decay content is low.
2. If Bandwidth is normal and Absorbance is normal then decay content is normal.
3. If Bandwidth is medium and Absorbance is medium then decay content is medium.
4. If Bandwidth is high and Absorbance is high then decay content is high and so on.

In the Fig.8 the Bandwidth is 423nm and Absorbance is 1.76nm then the corresponding decay content is 5.21ppm. The Fuzzy logic results and spectrophotometer results are compared in Table 2. The three dimensional graph in Fig.9 shows the variation of the Bandwidth to Absorbance and Decay contents. It shows the transformer oil samples different aging. From blue to yellow the graph shows that when the Absorbance of the transformer oil starts increasing the dissolve decay contents are increased accordingly and shows the aging of the transformer.

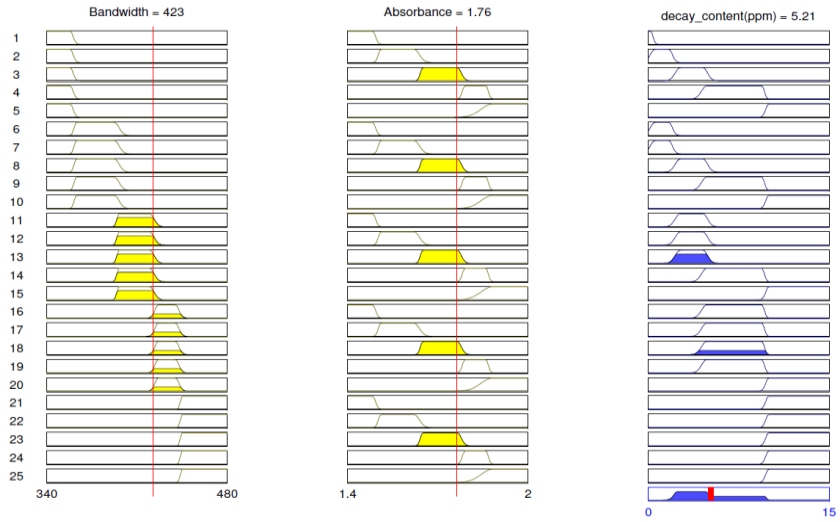

Fig.8 Fuzzy rules-Spectrophotometer decay content model

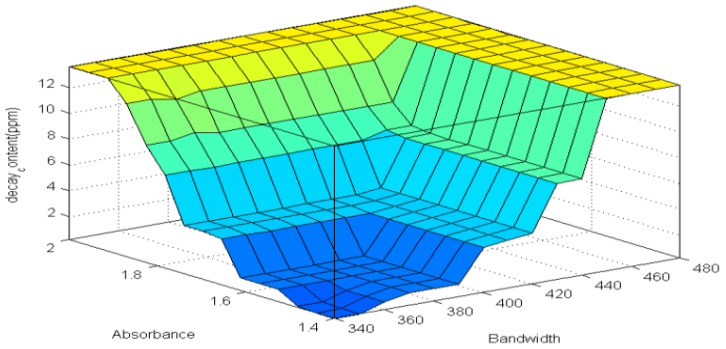

Fig. 9 Three dimensional mapping from bandwidth and absorption peak to decay content

The ANN simulation results are graphically shown in Fig. 10 to Fig13. The performance curve is shown in Fig.10. Mean Squared Error is the average squared difference between outputs and targets. Lower values are better. Zero means no error. In this figure mean squared error have become small by increasing the number of epoch. The best validation performance is 1.0054 at epoch 5. It means that target has tracked the output very efficiently.

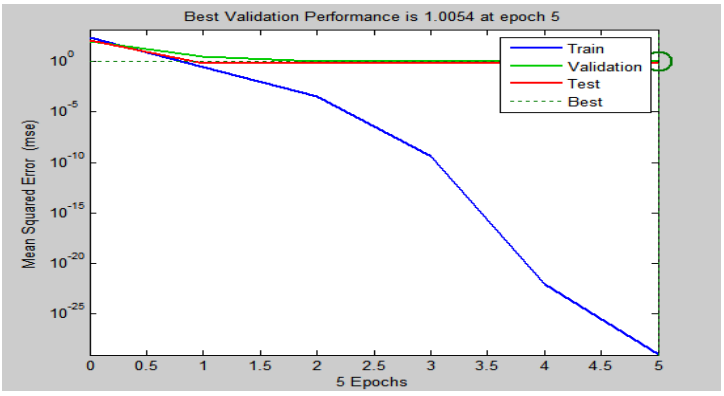

Fig.10 Mean Square Error of ANN model

.

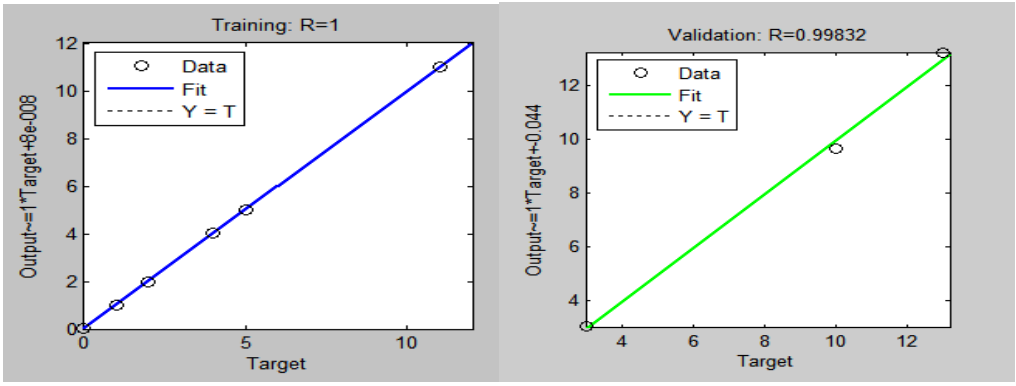

Fig.11 Prediction of Dissolve decay contents during training and validation analysis

During training of the output dissolve decay content is shown in Fig.11. These data are presented to the network during training, and the network is adjusted according to its error. As it can be seen that regression is equal to one which indicates close relation between target and output. The validations are used to measure network generalization, and to halt training when generalization stops improving**.** The validation regression plot is shown in Fig.11 and value of R is over 0.99.

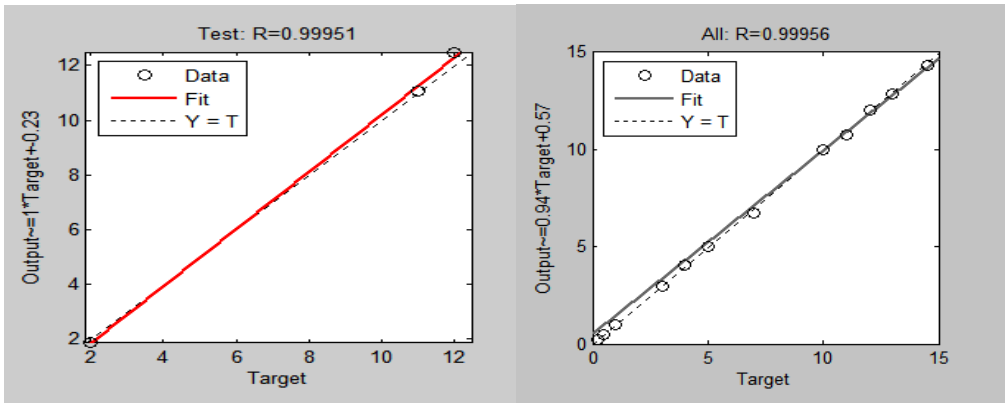

Fig.12 Prediction of Dissolve decay contents during testing analysis and during regression

The testing plot is shown in Fig.12. These have no effect on training and it provides an independent measure of network performance during and after training and the value of Regression R is 0.99951. The Regression plot is shown in Fig.12 its values measure the correlation between outputs and targets. If the value of R is 1 means a close relationship between target and output and if value of R is 0 then there is a random relationship between target and output of ANN.

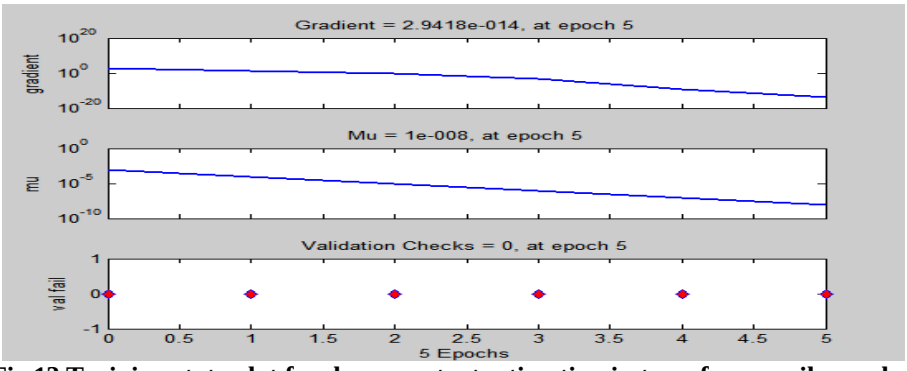

Fig.13 Training state plot for decay content estimation in transformer oil samples

The training state plot for dissolve decay content estimation is shown in Fig.13, it is seen that the training, validation, testing and regression plots all are over 0.999. Which shows a good response between the

output and targets which are selected. Hence, it is seen that the output of the ANN has tracked the dissolve decay content very well.

VI. Conclusion

Power transformers are very important in the transmission and distribution system. Hence the monitoring and diagnosis is very important for it. In this paper the Spectrophotometer method is used to detect the dissolve decay contents in transformer oil for replacement of the transformer oil. The UV spectrophotometer response of transformer oil can be measured instantly using relatively cheap equipment with no need to an expert person to perform the test. Results show that there is a relationship between dissolve decay content in transformer oil and its spectral response parameters with bandwidth and absorption. The paper introduces a novel fuzzy logic and ANN approach to estimate the transformer expected remnant life and used to find this relationship mathematically. It is found from comparison that all the results obtained from Fuzzy logic is almost equal with an accuracy of over 95% and ANN with an accuracy more than 99% as obtained from the UV spectrophotometer.

VII. Acknowledgements

The authors are thankful to the Technology Information Forecasting and Assessment Council and Centres of Relevance & Excellence (TIFAC-CORE) at NIT Hamirpur for providing the necessary facilities to perform the research work. And the authors are also thankful to the Himachal Pradesh Electricity Board (HPSEB), India for providing the transformer oil samples for experiment.

References

[1] T. K. Saha, "Review of Modern Diagnostic techniques for Assessing Insulation Condition Aged Transformers," IEEE Transaction on Dielectrics and Electrical Insulation, vol. 10, pp. 903-917, 2003.
[2] Hasmat Malik, A.Z and S.M, "Artificial Intelligence Techniques for Incipient Faults Diagnosis and Condition Assessment in Transformer" in Proc. Inter. Conf. on Emerging Trends in Engineering ISBN 978-93-81195-07-9, 2011, pp.5-8.
[3] ASTM D6802-02 (Reapproved 2010) standards; "Test Method for Determination of the Relative Content of Dissolved Decay Products in Mineral Insulating Oils by Spectrophotometry".
[4] Manual T90/T90+ "UV/VIS Spectrophotometer" [PG Instrument] TIFAC-CORE "NIT-HAMIRPUR.
[5] U. Mohan Rao, A.Pramoda & D.Vijay Kumar, "Decision Tree Based UV/VIS Response To Access the age of Transformer Oil" International Journal of Power System Operation and Energy Management, ISSN (PRINT): 2231–4407, Volume-1, Issue-2, 2011.
[6] MATLAB R2009b version 7.9.0.529.
[7] A. Abu-Siada, Lai Sin Pin, and Syed Islam, "Remnant Life Estimation of Power Transformer using Oil UV Vis Spectral Responses" Paper accepted for presentation at IEEE PSCE 09 that held in USA, March, 2009.
[8] S. M. Islam, T. Wu, G. Ledwich, "A Novel Fuzzy Logic Approach to Transformer Fault Diagnosis," IEEE Transaction on Dielectric and Electrical Insulation, Vol.7 No. 2,April 2000, pp. 177-186.
[9] A.Abu-Siada, M. Arshad, and S. Islam, "Fuzzy Logic Approach to Identify Transformer Criticality using Dissolved Gas Analysis," 978-1-4244-6551-4/10/©2010 IEEE.
[10] Hasmat Malik, S.M, R.K. Jarial, YRS, "Application and Implementation of Artificial Intelligence in Electrical System" published in international conference on Advances in Computing & Communication (ICACC-2011) ISBN 978-81-920874-0-5, Sponsored by IEEE-MTTS, pp. 499-505.
[11] Michael Negnevitsky "Artificial Intelligence A Guide to Intelligent Systems Second" Pearson Education Limited 2002.

Dr.Ashwani Kumar Chandel graduated in Electrical Engineering from Kerala University. He post graduated from Punjab Engineering College (PEC) Chandigarh. He was awarded Ph.D. degree from Indian Institute of Technology (IIT), Roorkee, India in 2005. Dr. Kumar joined Department of Electrical Engineering, National Institute of Technology, Hamirpur, HP, India, as faculty in 1991, where presently he is working as an Associate Professor and networking coordinator. His research work has been published in various International Journals of repute including IEEE, IEE, Elsevier Science, Taylor & Francis and others. He has worked extensively in the area of harmonic estimation & elimination and currently his interest continues in this field. He is a life member of ISTE (I).

Satyaprakash Ram graduated in Electrical Engineering from Government College Of Engineering Chandrapur, Maharashtra in the year 2009. He is currently pursuing his M.Tech in Condition Monitoring Control and Protection of Electrical Apparatus from NIT Hamirpur, India. He has worked extensively in the area of the condition monitoring of the transformer.

Gurmeet Singh graduated in Electrical and Electronics Engineering from College Of Engineering Roorkee in the year 2009. He is currently pursuing his M.Tech in Condition Monitoring Control and Protection of Electrical Apparatus from NIT Hamirpur, India.

Mithun Mondal graduated in Electrical and Electronics Engineering from Dr. M.G.R Engineering College, Chennai in the year 2009. He is currently pursuing his M.Tech in Condition Monitoring Control and Protection of Electrical Apparatus from NIT Hamirpur, India.